









Comprehensive thermodynamic study of three Co(II)- and Fe(II)-based octacyanonionobates

R. Pełka ^{1,*}, P. Konieczny ¹, Y. Miyazaki ², Y. Nakazawa ², T. Wasiutyński ¹, A. Budziak ³,
D. Pinkowicz ⁴ and B. Sieklucka ⁴¹The H. Niewodniczański Institute of Nuclear Physics, Polish Academy of Sciences, Radzikowskiego 152, 31-342 Kraków, Poland²Research Center for Thermal and Entropic Science, Graduate School of Science, Osaka University, Toyonaka, Osaka 560-0043, Japan³Department of Hydrogen Energy, Faculty of Energy and Fuels, AGH University of Science and Technology, al. Mickiewicza 30, Kraków, Poland⁴Faculty of Chemistry, Jagiellonian University, Ingardena 3, 30-060 Kraków, Poland

(Received 12 October 2021; accepted 22 November 2021; published 20 December 2021)

A comprehensive study of thermodynamic properties of three samples of bimetallic molecular magnets $[\text{Co}^{\text{II}}(\text{pyrazole})_4]_{2x}[\text{Fe}^{\text{II}}(\text{pyrazole})_4]_{2(1-x)}[\text{Nb}^{\text{V}}(\text{CN})_8] \cdot 4\text{H}_2\text{O}$ with $x = 1$ (Co_2Nb), 0.5 (CoFeNb), and 0 (Fe_2Nb) is reported. The three samples display the same crystallographic structure crystallizing in the tetragonal system with space group $I4_1/a$. Their heat capacities are measured in the temperature range 0.36–100 K without applied field as well as in the field of $\mu_0 H = 0.1, 0.2, 0.5, 1, 2, 5,$ and 9 T. The results imply the presence of the second-order phase transitions to magnetically ordered phases at 4.87(8), 7.1(2), and 8.44(3) K for $x = 1, 0.5,$ and 0, respectively. The corresponding thermodynamic functions are analyzed to discuss the stability of the mixed compound and the magnetocaloric effect (MCE). The Gibbs energy of mixing is found to be positive but smaller in magnitude than the energy of thermal fluctuations indicating that the mixed sample is most probably metastable in the full detected temperature range. The enthalpy of mixing is negative, which points to favoring a direct neighborhood of the Co(II) and Fe(II) ions in the solid solution CoFeNb . The negative values of the entropy of mixing are explained by considering the enhanced rigidity of the crystal lattice of the solid solution sample. To extract the magnetic contribution to the heat capacity, an approach based on a reasonable frequency spectrum is adopted. Taking advantage of the in-field heat capacity measurements, MCE was described in terms of the isothermal entropy change ΔS_{M} and the adiabatic temperature change ΔT_{ad} . The magnitudes of these quantities are typical for the class of molecular magnets. The values of $|\Delta S_{\text{M}}|^{\text{max}}$ detected for $\mu_0 \Delta H = 5$ T amount to 7.04, 5.26, and 4.93 $\text{J K}^{-1} \text{mol}^{-1}$ for Co_2Nb , CoFeNb , and Fe_2Nb , respectively, and are on the order of those obtained for the same field change in the isostructural compounds. The values of ΔT_{ad} detected for $\mu_0 \Delta H = 5$ T amount to 4.16, 2.47, and 2.01 K for Co_2Nb , CoFeNb , and Fe_2Nb , respectively, and are larger or comparable with those observed for the isostructural compounds. Temperature dependences of exponent n , quantifying the field dependence of ΔS_{M} , display minima close to the transition temperatures, implying through their values that the studied compounds belong to the universality class of the three-dimensional Heisenberg model. The regeneration Ericsson cycles employing the studied compounds as the working substance were considered. Most surprisingly, the Ericsson cycle operating between the temperatures corresponding to the full width at half maximum of the $|\Delta S_{\text{M}}|$ signal ($T_{\text{C}}, T_{\text{H}}$) turns out to be totally ineffective. Through shifting the temperature of the hot reservoir T_{H} down to the temperature T_{max} corresponding to $|\Delta S_{\text{M}}|^{\text{max}}$, the coefficient of performance is rendered positive and comparable with that of the Carnot cycle. A detailed analysis indicates that the regeneration Ericsson cycle operating between T_{C} and T_{max} should be most efficient for the maximal studied value of the applied field ($=9$ T) with irrelevant differences between the studied compounds.

DOI: [10.1103/PhysRevB.104.214428](https://doi.org/10.1103/PhysRevB.104.214428)

I. INTRODUCTION

For almost three decades now, magnetic coordination networks have been given assiduous attention by both chemists and physicists, resulting in materials displaying a long-range magnetic order above room temperature [1–3]. Concerted efforts were focused on obtaining compounds displaying additional key features such as structural and electronic non-rigidity, noncentrosymmetry, chirality, host-guest behavior,

luminescence, and others. They bore fruit in an array of classes of multifunctional magnetic materials with porous magnets, magnetic sponges, charge-transfer complexes, spin crossover magnets, photomagnets [4–13], noncentrosymmetric and chiral magnets [9,10,12,14–18], luminescent magnets [19], or compounds exploiting the second-order magneto-optical or magnetochiral effects [12,14,17,18]. The quest for coordination networks or clusters endowed with technologically relevant functionalities is by no means completed. In this respect, the magnetocaloric effect (MCE) [20] ranks among the emerging potential applications in cryogenic devices. Furthermore, one of the little exploited strategies to

*Corresponding author: Robert.Pelka@ifj.edu.pl

obtain molecular magnetic materials is the synthesis of substitutional mixtures displaying properties smoothly interpolating between those of the pure compounds [21–24]. This report goes along this late line of research.

MCE, i.e., heating or cooling of a magnetic material following switching on or off of applied magnetic field in adiabatic conditions, is an area of intensive research due to the fact that magnetic refrigerators represent an environmentally friendly technology, dispensing with media associated with ozone depletion or greenhouse effect. Moreover, they were demonstrated to show an enhanced efficiency in comparison with conventional gas compression-expansion refrigerators [25]. Crucial progress in this field involved on the one hand a considerable enhancement of material performance mostly realized through giant MCE (GMCE) [26,27] and on the other hand the cost reduction through the replacement of rare earth elements by transition metal alloys [28]. However, despite that GMCE occurring in materials with first-order magnetostructural phase transitions secures a large magnetic entropy change ΔS_M , it has two important deficiencies. The first is the narrowness of the ΔS_M vs T curve, and the other is the presence of hysteresis leading to low operational frequencies and limited cooling power [refrigeration capacity (RC)]. The profile of isothermal entropy change $\Delta S_M(T)$ of materials undergoing the second-order phase transitions is by contrast more extended, albeit it is smaller in magnitude. What is more, thermal hysteresis is not exhibited by this class of materials. Therefore, a compromise between an optimal RC and the lack of thermal hysteresis makes them superior candidates for the development of magnetic cooling devices. Recent developments in MCE resulted in a technological solution where the magnetic entropy change ΔS_M is obtained by rotating a single crystal in a constant magnetic field [29–32]. This technique is confined to materials displaying considerable magnetic anisotropy. The rotating MCE (RMCE) introduces crucial improvement of magnetic cooling by obviating the need to move the single-crystal coolant in and out of a magnetic field or manipulate the field amplitude and replacing it by a much simpler feasible change of the crystal orientation in a stationary field. Balli *et al.* [33,34] devised a prototype of a rotary magnetic refrigerator which integrates a simple construction with high efficiency, originating from the operation at higher frequencies than employed in conventional MCE, and a lower energy consumption due to the use of permanent magnets [33–35]. However, the latter feature puts a limit to the maximum field which can be employed for this type of cooling <2 T. RMCE is a very young topic, which is expressed by exceptionally sparse subject literature concerning inorganic materials [29–34] as well as molecular compounds [36–39].

In the field of molecular magnetism, MCE has been investigated most for single molecule magnets whose large ground-state spin value promises a substantial entropic effect [40–45]. Further studies were devoted to molecular rings, forming a subclass of molecular magnets characterized by a typical cyclic shape and a dominant antiferromagnetic coupling between the metallic nearest neighbors [46]. Additionally, early studies of MCE associated with the second-order phase transition to a long-range magneti-

cally ordered state involved Prussian blue analogs [47–49]. Further examples refer to a bimetallic octacyanoniate $\{[M(\text{II})(\text{pyrazole})_4]_2[\text{Nb}(\text{IV})(\text{CN})_8] \cdot 4\text{H}_2\text{O}\}_n$ ($M = \text{Mn}, \text{Ni}$) isomorphous with the compounds under study [50,51], an interesting instance of a molecular sponge changing reversibly the ordering temperature and the coercive field upon hydration/dehydration [52], and the effect of hydrostatic pressure on MCE in Mn_2 -pyridazine- $[\text{Nb}(\text{CN})_8]$ [53].

In this paper, we consider three samples of bimetallic molecular magnets with the formula $[\text{Co}^{\text{II}}(\text{pyrazole})_4]_{2x} [\text{Fe}^{\text{II}}(\text{pyrazole})_4]_{2(1-x)} [\text{Nb}^{\text{IV}}(\text{CN})_8] \cdot 4\text{H}_2\text{O}$ (pyrazole is a five-membered ring ligand $\text{C}_3\text{H}_4\text{N}$), where $x = 1$ (Co_2Nb), $x = 0.5$ (CoFeNb), and $x = 0$ (Fe_2Nb) [54], where the middle compound represents a substitutional mixture of the two marginal ones referred to in what follows as the mixed and pure compounds, respectively. All three compounds are isostructural and crystallize in the tetragonal $I4_1/a$ space group. Their structure consists of a three-dimensional (3D) skeleton, where each Nb(IV) center is linked through the cyanido bridges $M(\text{II})\text{-NC-Nb}(\text{IV})$ to four $M(\text{II})$ ($M = \text{Co}, \text{Fe}$) ions, whereas each $M(\text{II})$ center is bridged exclusively to two Nb(IV) ions. The remaining part of the distorted pseudooctahedral coordination sphere of $M(\text{II})$ is filled with pyrazole molecules, while the Nb(IV) ion coordinates further four terminal CN^- ligands. The fact that such low connectivity indices should produce a 3D extended network represents the unique structural feature of these compounds. The graphical representation of the crystal structure of these compounds is shown in Fig. 1 for instant reference.

The pure compounds Co_2Nb and Fe_2Nb were demonstrated to undergo a magnetic transition to a long-range order state at 5.9(5) and 8.3(5) K, respectively, where the transition points were assumed to coincide with the position of the dM/dT peak [54,55]. The analysis of the DC susceptibility and isothermal magnetization carried out in the framework of the molecular field model suggested that the character of the exchange coupling between the Co(II) and Nb(IV) centers is ferromagnetic, while that between the Fe(II) and Nb(IV) ions is antiferromagnetic with the exchange coupling constants estimated to amount to $J_{\text{Co-Nb}} = +3.5(3) \text{ cm}^{-1}$, and $J_{\text{Fe-Nb}} = -3.1(2) \text{ cm}^{-1}$ [54,55]. Co_2Nb was thus found to be a molecular ferromagnet, whereas Fe_2Nb was found to be a molecular ferrimagnet. The critical behavior of Fe_2Nb studied with the use of AC magnetometry and zero-field μSR spectroscopy allowed us to determine the static critical exponents $\beta = 0.42(3)$, $\gamma = 1.38(8)$, and the dynamic exponent $w = 0.33(2)$, thus placing the compound in the universality class of the 3D Heisenberg model [56,57]. Moreover, preliminary measurements of Fe_2Nb by relaxation calorimetry in zero and nonzero applied fields were analyzed to extract temperature dependences of the isothermal entropy change ΔS_M and the adiabatic temperature change ΔT_{ad} due to the magnetic field change, the two basic characteristics of the MCE. Let us note that the approach to calculating the MCE characteristics was different than that reported here. The maximum value of ΔS_M for $\mu_0\Delta H = 5$ T was found to be placed at 10.3 K and amounts to $4.8 \text{ J mol}^{-1} \text{ K}^{-1}$, while the corresponding maximum value of $\Delta T_{\text{ad}} = 2$ K was observed at 8.9 K [58,59]. The thermodynamic properties of the other pure compound Co_2Nb

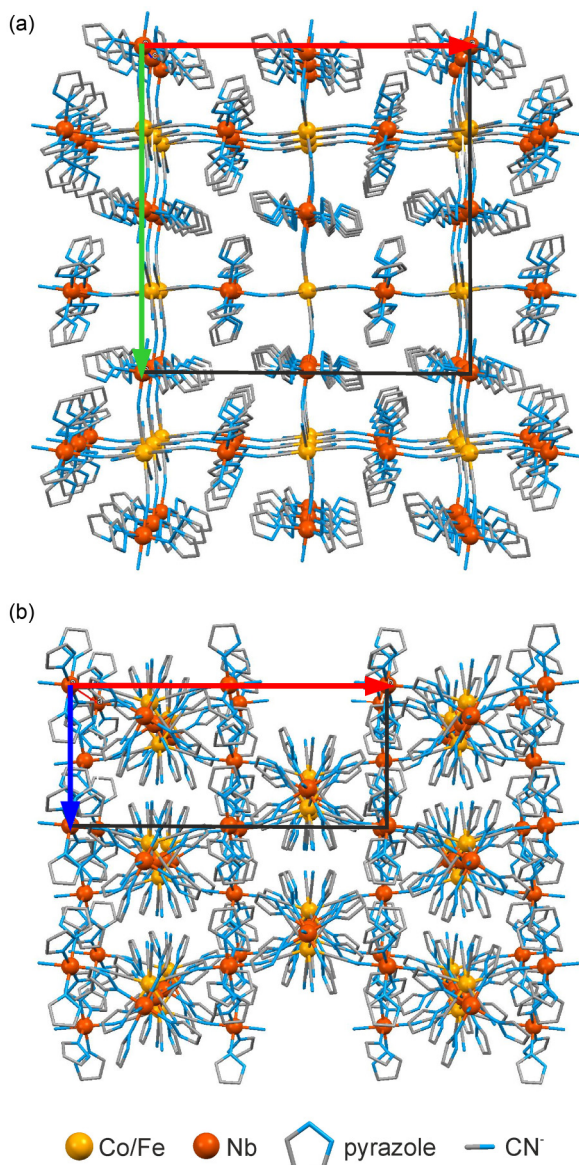


FIG. 1. Structure of $\{[M^{\text{II}}(\text{pyrazole})_4]_2[\text{Nb}^{\text{IV}}(\text{CN})_8] \cdot 4\text{H}_2\text{O}\}_n$. (a) View of the structure along the c crystallographic axis (red and green mark the a and b crystallographic axes, respectively). The water molecules and hydrogen atoms are not shown for clarity. (b) View of the structure along the b crystallographic axis (red and blue mark the a and c crystallographic axes, respectively).

as well as the mixed one CoFeNb have not been reported previously.

To study thermodynamic properties of the reported compounds, their heat capacities have been measured by relaxation calorimetry. The compounds are demonstrated to display transitions to magnetically long-range ordered states at 4.9 K (Co_2Nb), 7.3 K (CoFeNb), and 8.8 K (Fe_2Nb), as indicated by the positions at which the derivative $dC_p(T)/dT$ vanishes, revealing the local maxima of $C_p(T)$. The measured values of C_p are prerequisites of a detailed discussion of thermodynamic properties of the three samples with the focus on the mixed compound CoFeNb. This paper is organized as follows. On providing the experimental details in Sec. II, we analyze and

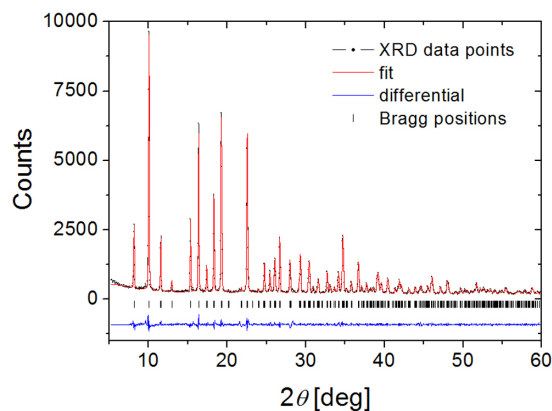


FIG. 2. Observed (symbols), calculated (solid line), and difference (observed-calculated; bottom solid line) x-ray diffraction profiles at 300 K for CoFeNb indicate the positions of the Bragg reflections for tetragonal phase with space group $I4_1/a$.

discuss the thermal behavior in zero applied field in Sec. III. Then in Sec. IV, we go on to describe an extraction procedure of the magnetic contribution to the heat capacity. Section V is devoted to the calculation and discussion of the MCE of the studied samples with some comments on its practical aspects. We close the paper in Sec. VI with general conclusions.

II. EXPERIMENTAL

The polycrystalline samples of Co_2Nb , Fe_2Nb were synthesized according to the procedures reported in Ref. [54], while the CoFeNb solid-state solution was synthesized according to a modified procedure. A solution of $(\text{NH}_4)_2\text{Fe}(\text{SO}_4)_2 \cdot 6\text{H}_2\text{O}$ (39 mg, 0.1 mmol), $\text{CoCl}_2 \cdot 6\text{H}_2\text{O}$ (23 mg, 0.1 mmol), and pyrazole (82 mg, 1.2 mmol) in degassed water (3 mL) was added dropwise to the degassed aqueous solution (3 mL) of $\text{K}_4\text{Nb}(\text{CN})_8 \cdot 2\text{H}_2\text{O}$ (50 mg, 0.1 mmol). A violet precipitate formed immediately. The suspension was stirred for 5 min, filtered, and dried shortly in air. The violet powder was stored at low temperature due to slight sensitivity to air.

The combustion analysis (C, H, N) was performed using an Elementar vario MICRO cube elemental analyzer. ICP-OES analysis (Co, Fe, Nb) was performed using a Perkin Elmer, ICP-OES Optima 2100D instrument (45.68 mg sample dissolved in aqueous EDTA solution). Analysis calculated for $\text{C}_{32}\text{CoFeH}_{40}\text{N}_{24}\text{NbO}_4$: C, 37.22; H, 3.90; Co, 5.71; Fe, 5.41; N, 32.56; Nb, 9.0. ICP-OES (Co, Fe, Nb) and combustion analysis (C, H, N) found: C, 36.82; H, 3.85; Co, 6.11; Fe, 5.82; N, 31.99; Nb, 8.7. The powder x-ray diffraction pattern for CoFeNb was recorded at room temperature using a PANalytical X'Pert PRO MPD diffractometer (Cu $K\alpha$ x-ray radiation 1.541874 Å). It was identified with the FULLPROF program [60] based on the Rietveld method [61]. The best fit was obtained with the assumption of a tetragonal structure identical to that for Co_2Nb , Fe_2Nb (space group: $I4_1/a$; lattice parameters: $a = 21.633(6)$ Å, $c = 9.619(4)$ Å; cell volume: 4501.6 Å³; R-factors, not corrected for background: $R_p = 4.79$, $R_{\text{wp}} = 6.61$, $R_{\text{exp}} = 4.70$, $\chi^2 = 1.97$), see Fig. 2. There were no traces of distortion or the second phase. For

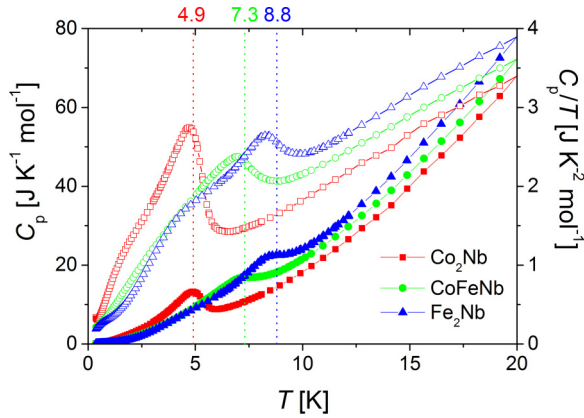


FIG. 3. Zero-field heat capacity in terms of C_p (full symbols) and C_p/T (open symbols) of the studied samples in the low-temperature regime.

the CoFeNb compound, it was not possible to distinguish the positions of Co and Fe atoms in the powder x-ray diffraction pattern, as they occupy the same $8c$ Wyckoff position [62].

The heat capacity measurements were carried out with the PPMS Quantum Design instrument by the relaxation calorimetry technique. The measurements were performed in two independent stages. In the high-temperature stage, using polycrystalline samples of mass 1.7504 mg (Co_2Nb), 2.2627 mg (CoFeNb), and 2.0087 mg (Fe_2Nb) pressed to form small pellets, the heat capacity was detected in the cooling direction in the temperature range of 1.9–101 K without applied field by the standard probe cooled with ^4He . In the low-temperature stage, employing the ^3He probe and using polycrystalline samples of mass 1.5417 mg (Co_2Nb), 2.4641 mg (CoFeNb), and 3.3189 mg (Fe_2Nb) pressed to form small pellets, the heat capacity measurements were run in the cooling direction in the temperature range of 0.36–20.2 K without applied field as well as in the field of $\mu_0 H = 0.1, 0.2, 0.5, 1, 2, 5, \text{ and } 9$ T. Since the heat capacity data measured with the ^3He system at high temperatures and the data detected with the ^4He system at low temperatures are generally incorrect, we decided to use the zero-field data provided by the former system < 20 K and those provided by the latter system > 20 K.

III. ZERO-FIELD HEAT CAPACITY

In the beginning, let us focus on the zero-field data. Figure 3 shows the zero-field heat capacity in the range 0.36–20 K for the studied samples. All three samples reveal anomalies which can be assigned to the second-order phase transition to a magnetically ordered phase. The transition temperatures of the compounds are 4.9 K (Co_2Nb), 7.3 K (CoFeNb), and 8.8 K (Fe_2Nb), as indicated by the positions at which the derivative $dC_p(T)/dT$ vanishes, revealing the local maxima of $C_p(T)$. The uncertainty related to these values was estimated to amount to 0.1 K. Let us stress that, for the mixed compound CoFeNb , we observe a single anomaly with the transition temperature placed between the transition temperatures of the pure samples Co_2Nb and Fe_2Nb , which implies that the sample is a single-phase one with the metal sites occupied randomly by the Co(II) and Fe(II) ions according

TABLE I. Constituent metal nuclei [63].

Nucleus	Spin quantum number I	Abundance (%)
^{59}Co	$\frac{7}{2}$	100
^{54}Fe	0	5.845
^{56}Fe	0	91.754
^{57}Fe	$\frac{1}{2}$	2.119
^{58}Fe	0	0.282
^{93}Nb	$\frac{9}{2}$	100

to the expected ratio 1:1 (a proper mixture), and thus, no phase decomposition takes place. Moreover, the transition temperature of CoFeNb compares well with the value of 7.1 K predicted by the molecular field model, see Eq. (A7) in the Appendix.

The following analysis aims to calculate consistently the thermodynamic functions based on the heat capacity data. To do it correctly, one needs the extrapolation of the heat capacity data in the experimentally missing temperature interval of 0–0.36 K. The correct extrapolation must consider the nuclear contributions to the heat capacity. Table I shows the spin states together with the abundances of the constituent nuclei.

It thus turns out that we must account for the nonzero nuclear spin of the Co and Nb ions, while the nuclear contribution of the Fe ion may be safely neglected. To quantify the nuclear contribution to the heat capacity, we assume that the ground state of either nucleus is split due to the local magnetic field. The energy of this splitting is given by the following formula:

$$E(M_I) = AM_I(M_I - I, -I + 1, \dots, I - 1, I),$$

where A (in units of energy) is proportional to the local field strength, and I denotes the nuclear spin quantum number. The corresponding contribution to the molar specific heat has the following form:

$$C_n(\beta; A, I) = \frac{1}{4}R(\beta A)^2 \left[4I(I+1) - (2I+1)^2 \text{ctgh}^2\left(\frac{2I+1}{2}\beta A\right) + \text{ctgh}^2\left(\frac{\beta A}{2}\right) \right], \quad (1)$$

where $\beta = 1/k_B T$. Apart from the contribution from the nuclear magnetism, at low temperatures, we expect a contribution from the ionic magnetism and lattice vibrations. The former involves the effects due to the long-range order (magnons), the interaction with the local magnetic field present in the ordered phase, and the hyperfine interaction of the ionic spins. In addition, we expect the hyperfine field to be lower than the local field due to the long-range order, and additionally, the corresponding heat capacity contribution is expected to be substantially altered by the long-range correlations. All these effects give rise to a single correlated contribution, which we assume to be an increasing function of temperature. Likewise, the lattice contribution is expected to be an increasing function of temperature. We therefore represent the contribution from the ionic magnetism and lattice vibrations by a single algebraic term BT^C . Thus, the

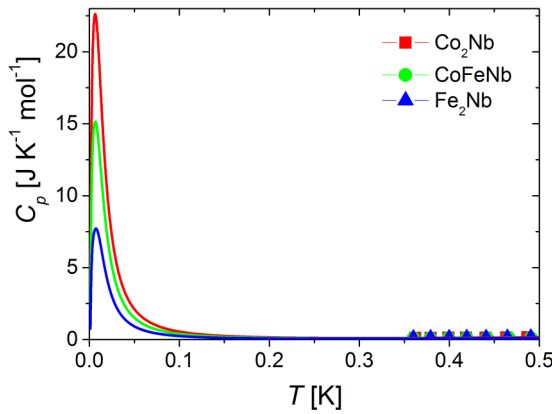


FIG. 4. Extrapolation of the zero-field heat capacity data down to 0 K. The Schottky anomalies corresponding to the nuclear magnetism of the samples are apparent.

low-temperature molar specific heat of the samples takes on the following form:

$$C_{LT}(\text{Co}_2\text{Nb}) = 2C_n(\beta; A_{\text{Co}}, \frac{7}{2}) + C_n(\beta; A_{\text{Nb}}, \frac{9}{2}) + B_1 T^{C_1}, \quad (2)$$

$$C_{LT}(\text{CoFeNb}) = C_n(\beta; A_{\text{Co}}, \frac{7}{2}) + C_n(\beta; A_{\text{Nb}}, \frac{9}{2}) + B_2 T^{C_2}, \quad (3)$$

$$C_{LT}(\text{Fe}_2\text{Nb}) = C_n(\beta; A_{\text{Nb}}, \frac{9}{2}) + B_3 T^{C_3}, \quad (4)$$

where B_i and C_i ($i = 1, 2, 3$) are the coefficients of the algebraic term corresponding to the three compounds under study, respectively. We performed a simultaneous fit of the formulas in Eqs. (2)–(4) to the experimental data within the temperature range 0.36–0.75 K with all parameters A_{Co} , A_{Nb} , B_i , C_i ($i = 1, 2, 3$) relaxed, but this implied unacceptable errors for quantities A_{Co} and A_{Nb} . It was only after assuming that $A_{\text{Co}} = A_{\text{Nb}} = \bar{A}$ that the fit was perfectly convergent, yielding $A_{\text{Co}} = A_{\text{Nb}} = \bar{A} = 0.0060(3)\text{K}$, $B_1 = 0.70(1)\text{J K}^{-1}\text{mol}^{-1}$, $C_1 = 2.27(5)$, $B_2 = 0.42(1)\text{J K}^{-1}\text{mol}^{-1}$, $C_2 = 2.05(6)$, $B_3 = 0.366(8)\text{J K}^{-1}\text{mol}^{-1}$, $C_3 = 1.84(5)$. The values of exponents C_i ($i = 1, 2, 3$) are placed between 1.5 and 3, which might be expected for the temperature interval <1 K, where the magnetic contribution ($\sim T^{3/2}$) dominates the lattice contribution ($\sim T^3$). Furthermore, using the fitted value of \bar{A} and employing the relation

$$B_{\text{int}} = \frac{k_B \bar{A}(K) I}{\mu(\mu_N) \mu_N \left(\frac{J}{T}\right)}, \quad (5)$$

where $\mu_N = 5.050783699(31) \times 10^{-27}\text{J T}^{-1}$ is the nuclear magneton [64], and μ is the nuclear moment expressed in nuclear magnetons ($\mu_{\text{Co}} = 4.627(9)$, $\mu_{\text{Nb}} = 6.1705(3)$ [65]), one can estimate the magnitude of the local magnetic field. One hence obtains $B_{\text{int,Co}} = 12.4(6)$ T at the Co nucleus and $B_{\text{int,Nb}} = 12.0(6)$ T at the Nb nucleus, both of which are on the plausible order of magnitude. Thus, it may be concluded that the extrapolation of the heat capacities down to 0 K is credible. Figure 4 shows the result of the extrapolation. The Schottky anomalies corresponding to the nuclear magnetism of the samples are apparent.

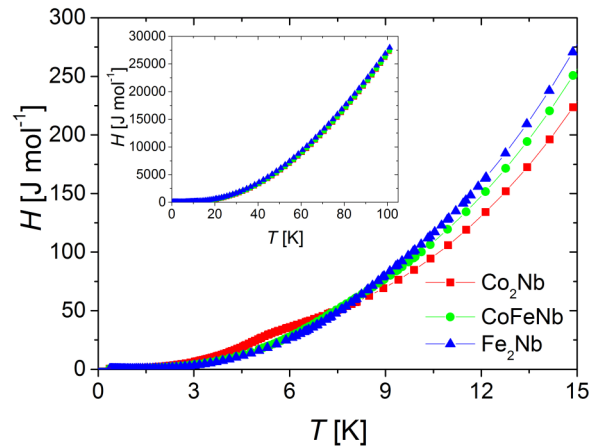


FIG. 5. Temperature dependence of the enthalpies of the studied samples. Inset: The full range data.

Now that the extrapolations are ready to use, we can determine the thermodynamic functions. They were numerically calculated using the following formulas:

$$H(T) = \int_0^T C_p(T') dT', \quad (6)$$

$$S(T) = \int_0^T \frac{C_p(T')}{T'} dT', \quad (7)$$

$$G(T) = H(T) - TS(T), \quad (8)$$

where C_p denotes the molar specific heat, H the enthalpy, S the entropy, and G the Gibbs free energy. Figures 5–7 show the temperature dependence of the enthalpies, entropies, and the Gibbs free energies of the studied compounds, respectively.

Figure 7 shows the closeup of the Gibbs free energies of the studied samples. The points corresponding to the mixed sample CoFeNb are placed in between the points corresponding to the pure compounds Co₂Nb and Fe₂Nb, which might have been expected. The black solid line shows the value of the equally weighted average of the Gibbs energies of the pure compounds: $G_{\text{avg}} = [G(\text{Co}_2\text{Nb}) + G(\text{Fe}_2\text{Nb})]/2$. The points of the mixed sample (green circles) lie slightly above the black

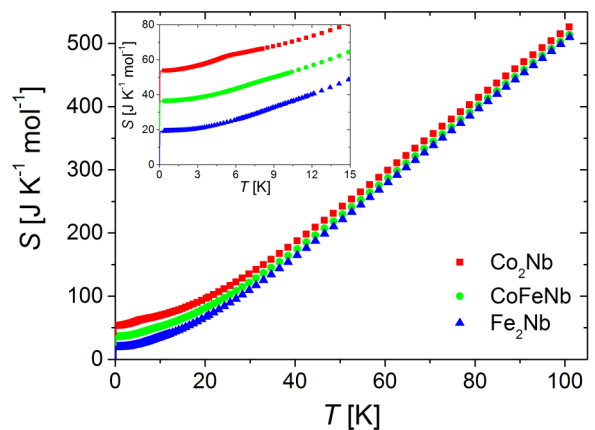


FIG. 6. Temperature dependence of the entropies of the studied samples. Inset: The low-temperature closeup.

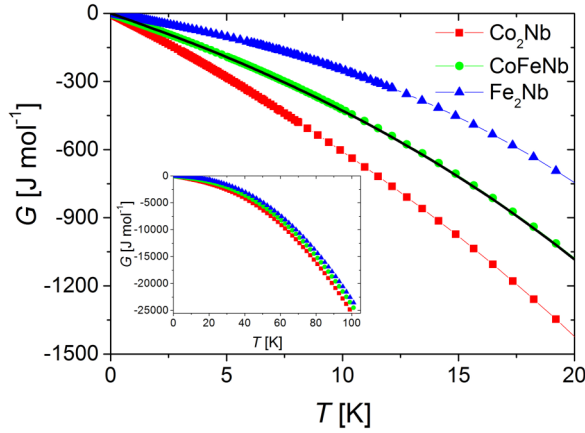


FIG. 7. Temperature dependence of the Gibbs free energies of the studied samples. Inset: The full range data.

curve, indicating that there is a positive excess Gibbs energy. Figure 8 shows the temperature dependence of the excess Gibbs energy $\Delta G_{\text{mix}} = G(\text{CoFeNb}) - G_{\text{avg}}$, the excess enthalpy $\Delta H_{\text{mix}} = H(\text{CoFeNb}) - H_{\text{avg}}$, and the excess entropy $\Delta S_{\text{mix}} = S(\text{CoFeNb}) - S_{\text{avg}}$, which can be interpreted as the Gibbs free energy, the enthalpy, and the entropy of mixing, respectively.

Indeed, the Gibbs free energy of mixing ΔG_{mix} is positive in the full temperature range, which suggests that there is an additional energy input in the mixed sample CoFeNb compared with the pure ones. This excess energy is most probably due to a slight misfit of the two different ions accommodated in a single crystal structure [62]. For the sake of argument, let us express the value of ΔG_{mix} observed at 100 K in terms of temperature, i.e., $\Delta T_{\text{mix}} = \Delta G_{\text{mix}}/R$, where $R = 8.3144598(48) \text{ J K}^{-1} \text{ mol}^{-1}$ is the molar gas constant [64]. One readily obtains that $\Delta T_{\text{mix}} = 25.8 \text{ K}$, which is one order of magnitude lower than the average energy of thermal fluctuations at that temperature (100 K). With $G(\text{CoFeNb}) > [G(\text{Co}_2\text{Nb}) + G(\text{Fe}_2\text{Nb})]/2$ ($\Delta G_{\text{mix}} > 0$), the mixed sample resides most probably in some metastable state with the energy barrier exceeding the energy of thermal fluctuations and preventing the system from phase separation. It

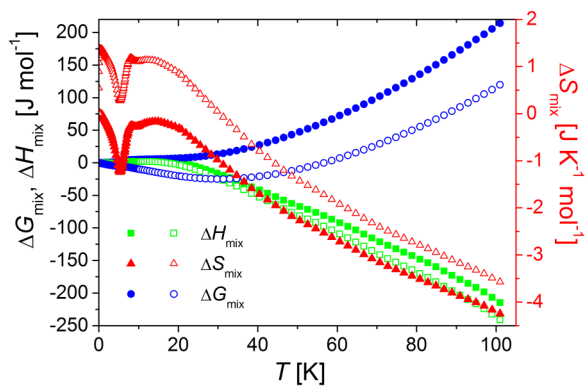


FIG. 8. Temperature dependence of the excess Gibbs free energy, the excess enthalpy, and the excess entropy of the solid-state solution CoFeNb (solid symbols) and the unbalanced composition corresponding to $x = 0.46$ (open symbols).

could seem that the situation would change if we used the experimental value of the population fraction x , but it is not the case. Moreover, the combustion analysis of the key transition elements Co and Fe implies ambiguous values for $x = 0.54$ and 0.46 , respectively. It can be admittedly shown that ΔG_{mix} becomes negative in the limited interval of low temperatures for $x = 0.46$; however, its depth does not exceed -25 J mol^{-1} , and it displays an increasing trend with positive values $> 60 \text{ K}$ again (see open symbols in Fig. 8).

At the same time, the enthalpy of mixing ΔH_{mix} is negative in the full temperature range. To understand the implications of this fact, let us assume that there are N lattice sites in the crystal structure on which substitution takes place, and each such lattice site is surrounded by z nearest neighboring sites belonging to this set. Then the total number of the nearest-neighbor bonds is $\frac{1}{2}Nz$, where the factor $\frac{1}{2}$ arises since there are two ions per bond. Next, let the energy associated with Co-Co, Fe-Fe, and Co-Fe nearest-neighbor pairs be, respectively, E_{CoCo} , E_{FeFe} , and E_{CoFe} . If the Co and Fe ions are mixed randomly, then the probability of Co-Co, Fe-Fe, and Co-Fe neighbors is x^2 , $(1-x)^2$, and $2x(1-x)$, respectively, where x denotes the mole fraction of the Co ions. Hence, the total enthalpy of the solid solution is given by

$$H = \frac{1}{2}Nz[x^2E_{\text{CoCo}} + (1-x)^2E_{\text{FeFe}} + 2x(1-x)E_{\text{CoFe}}], \quad (9)$$

which can be rearranged to read

$$H = \frac{1}{2}Nz[xE_{\text{CoCo}} + (1-x)E_{\text{FeFe}}] + \frac{1}{2}Nzx(1-x)(2E_{\text{CoFe}} - E_{\text{CoCo}} - E_{\text{FeFe}}). \quad (10)$$

The first term in Eq. (10) corresponds to the enthalpy of the mechanical mixture, while the second term may be interpreted as the excess enthalpy of mixing ΔH_{mix} . Its sign is determined by the sign of the interaction parameter $E_{\text{int}} = 2E_{\text{CoFe}} - E_{\text{CoCo}} - E_{\text{FeFe}}$. The negative value of E_{int} ($E_{\text{CoFe}} < (E_{\text{CoCo}} + E_{\text{FeFe}})/2$), which is the case with CoFeNb ($\Delta H_{\text{mix}} < 0$), indicates that it is energetically more favorable to have Co-Fe neighbors rather than Co-Co or Fe-Fe neighbors. To minimize the internal energy of the compound, the number of Co-Fe neighbors should be maximized; thus, the mixing is favored in the solid solution.

Although the negative values of the enthalpy of mixing ΔH_{mix} can be understood in terms of fostering a mixed arrangement of the Co and Fe ions in the solid solution CoFeNb, the fact that the excess entropy ΔS_{mix} is also negative in the full temperature range is more surprising and more challenging to rationalize. Assuming that the entropy of the solid solution is mainly vibrational in origin, i.e., related to the structural disorder caused by thermal vibrations of the atoms at finite temperature, let us consider a toy model of a one-dimensional lattice whose sites may be occupied by two types of atoms A and B. The pure compounds Co_2Nb and Fe_2Nb correspond to the configurations where the sites are occupied exclusively either by A- or B-type atoms, while the solid solution CoFeNb is tantamount to the configuration where there are exactly as many A- as B-type atoms in the system, and either they are randomly distributed over the lattice sites, or their distribution is ordered with an alternating arrangement of the atoms forming the $\dots\text{ABABAB}\dots$ chain. Figure 9 shows the four different configurations.

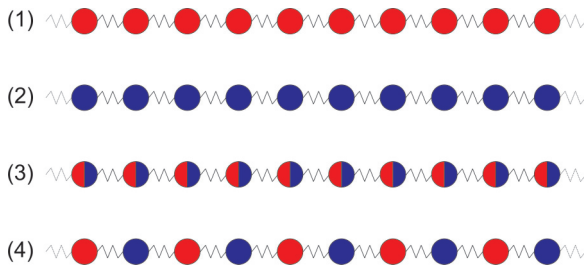


FIG. 9. The four different configurations of the one-dimensional lattice considered in the toy model. (1) The configuration corresponding to the pure compound Co_2Nb . (2) The configuration corresponding to the pure compound Fe_2Nb . (3) The configuration corresponding to the solid solution CoFeNb with the disordered distribution of the constituent atoms. (4) The configuration corresponding to the solid solution CoFeNb with the ordered distribution of the constituent atoms.

For configurations (1)–(3), the lattice involves a monoatomic basis with atoms of mass m_1 , m_2 , and $(m_1 + m_2)/2$ (the equally weighted mean of the masses of the individual atoms), respectively. The corresponding phonon spectrum is defined by the following dispersion relation:

$$\omega^{(i)}(ka) = 2\sqrt{\frac{k_f}{m^{(i)}}} \left| \sin\left(\frac{1}{2}ka\right) \right| \quad \text{with} \\ -\pi \leq ka \leq \pi \quad (i = 1, 2, 3), \quad (11)$$

where k_f is the force constant, $m^{(i)}$ is the mass of the atom, k is the wave vector, and a is the distance between the nearest neighbors (the lattice constant). The basis of the lattice configuration (4) is diatomic (there is an alternating arrangement of atoms of mass m_1 and m_2), which leads to the presence of two branches in the phonon spectrum with the following dispersion relation:

$$\omega_{\pm}^{(4)}(ka) = \sqrt{\frac{k_f}{\mu}} \sqrt{1 \pm \sqrt{1 - 4\left(\frac{\mu}{m}\right)^2 \sin^2(ka)}} \quad \text{with} \\ -\frac{\pi}{2} \leq ka \leq \frac{\pi}{2}, \quad (12)$$

where $+$ corresponds to the optical branch, while $-$ to the acoustic branch, $\mu = m_1 m_2 / (m_1 + m_2)$, $m = \sqrt{m_1 m_2}$, and a is still the distance between the nearest neighbors (the lattice constant being now $2a$). Knowing that the entropy associated with a single phonon mode of circular frequency ω at temperature T is given by the formula

$$\frac{S_{\text{vib}}(\omega)}{k_B} = \frac{\beta \hbar \omega}{e^{\beta \hbar \omega} - 1} - \ln(1 - e^{-\beta \hbar \omega}), \quad (13)$$

where $\beta = 1/k_B T$, one can calculate the molar vibrational entropy of the four lattice configurations in the continuous limit using the formulas

$$\frac{S_{\text{vib}}^{(i)}}{R} = \frac{3}{2\pi} \int_{-\pi}^{\pi} d\xi S_{\text{vib}}[\omega^{(i)}(\xi)] \quad (i = 1, 2, 3), \quad (14)$$

$$\frac{S_{\text{vib}}^{(4)}}{R} = \frac{3}{2\pi} \int_{-\pi/2}^{\pi/2} d\xi \{S_{\text{vib}}[\omega_+(\xi)] + S_{\text{vib}}[\omega_-(\xi)]\}, \quad (15)$$

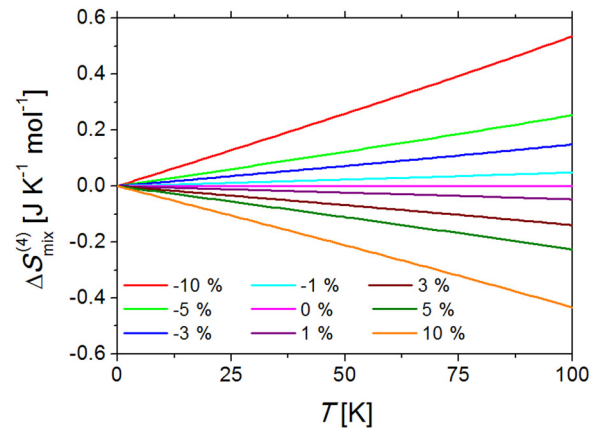


FIG. 10. The temperature dependence of $\Delta S_{\text{mix}}^{(4)}(\delta)$ for several indicated values of δ . It is apparent that stiffening of the lattice ($\delta > 0$) leads to negative values of the entropy of mixing.

where R is the molar gas constant, and factor 3 accounts for one longitudinal and two transverse modes. Assuming $m_1 = m_{\text{Co}} = 58.933194u$, $m_2 = m_{\text{Fe}} = 55.845u$ [64], $k_f = 520 \text{ N m}^{-1}$ (typical for a single bond like in HCl), which returns the reference energy scale of lattice vibrations $T_{\text{vib},0} = \hbar\sqrt{k_f/\mu}/k_B = 800 \text{ K}$, and allowing for a change of $T_{\text{vib}} = T_{\text{vib},0}[1 + \delta(\%) / 100]$ within some range for mixed configurations (3) and (4), as induced by a possible change of the force constant k_f , we calculated the corresponding entropies of mixing defined by

$$\Delta S_{\text{mix}}^{(j)}(\delta) = S_{\text{vib}}^{(j)}(\delta) - \frac{S_{\text{vib}}^{(1)} + S_{\text{vib}}^{(2)}}{2} \quad (j = 3, 4). \quad (16)$$

Figure 10 shows the temperature dependence of $\Delta S_{\text{mix}}^{(4)}(\delta)$ for an array of values of $\delta = -10, -5, -3, -1, 0, 1, 3, 5$, and 10% [a similar plot for $\Delta S_{\text{mix}}^{(3)}(\delta)$ is not shown for being almost the same]. Stiffening of the lattice ($\delta > 0$), which may be due to the requirement of accommodating two different atoms within the same lattice structure, leads to negative values of the entropy of mixing. This is most probably the case with our solid solution sample CoFeNb .

Finally, we want to analyze the entropy content of the studied samples associated with the discrete degrees of freedom, i.e., nuclear and ionic spins. For this purpose, we choose to look at the entropy differences between the samples, assuming that the lattice contributions in all three cases are comparable and will cancel each other out if we take duly into account the entropy of mixing for CoFeNb , which was shown above to be vibrational in origin. Figure 11 shows the result of the subtractions.

All three differences indicated in Fig. 11 were constructed to reveal positive values in the whole temperature range. The differences are peaked at low temperatures, which is associated with the entropy contributions originating from the nuclear spins $S_n(\text{Co}) = R \ln(2 \times 7/2 + 1) \approx 17.29 \text{ J K}^{-1} \text{ mol}^{-1}$ and $S_n(\text{Nb}) = R \ln(2 \times 9/2 + 1) \approx 19.14 \text{ J K}^{-1} \text{ mol}^{-1}$; with $S_n(\text{Co}_2\text{Nb}) \approx 2S_n(\text{Co}) + S_n(\text{Nb})$, $S_n(\text{Fe}_2\text{Nb}) \approx S_n(\text{Nb})$, and $S_n(\text{CoFeNb}) \approx S_n(\text{Co}) + S_n(\text{Nb})$, one arrives at $S_n(\text{Co}_2\text{Nb}) - S_n(\text{Fe}_2\text{Nb}) \approx 2S_n(\text{Co}) \approx$

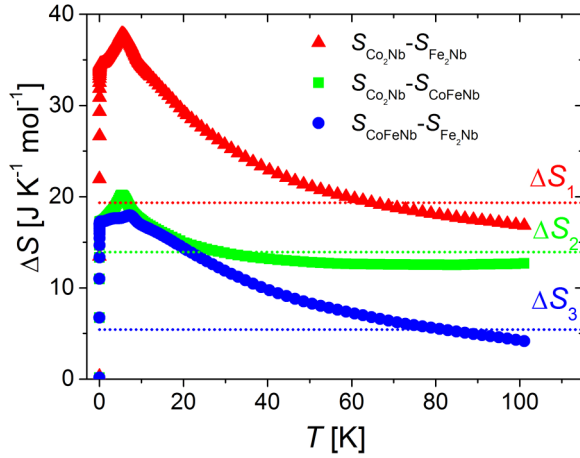


FIG. 11. Temperature dependence of the entropy differences between the studied samples.

$34.58 \text{ J K}^{-1} \text{ mol}^{-1}$, $S_n(\text{Co}_2\text{Nb}) - S_n(\text{CoFeNb}) \approx S_n(\text{Co}) \approx 17.29 \text{ J K}^{-1} \text{ mol}^{-1}$, and $S_n(\text{CoFeNb}) - S_n(\text{Fe}_2\text{Nb}) \approx S_n(\text{Co}) \approx 17.29 \text{ J K}^{-1} \text{ mol}^{-1}$, which is roughly consistent with the peak heights. With increasing temperature, the differences decrease and approach something close to saturation at the high-temperature limit, which should be so if the lattice contributions should cancel out. We can estimate the values of the entropy differences expected at high temperatures by assuming that the ionic spin contributions are saturated there. The spin of the Fe(II) ion is $S_{\text{Fe}} = 2$, the spin of the Nb(IV) ion amounts to $S_{\text{Nb}} = \frac{1}{2}$, while the spin of the Co(II) ion is taken to be equal to $S_{\text{Co}} = \frac{1}{2}$, as we assume that, $<100 \text{ K}$, essentially only the ground state of the Co(II) ion is populated, which is the Kramers doublet originating from the crystal-field split multiplet corresponding to the full spin of $\frac{3}{2}$. One thus obtains

$$\begin{aligned} S_{\text{Co}_2\text{Nb}} &= S_0 + R[2 \ln(2S_{\text{Co}} + 1) + \ln(2S_{\text{Nb}} + 1)] \\ &\quad + 2S_n(\text{Co}) + S_n(\text{Nb}) \\ &\approx 71.01 \text{ J K}^{-1} \text{ mol}^{-1}, \end{aligned} \quad (17)$$

$$\begin{aligned} S_{\text{CoFeNb}} &= S_0 + R[\ln(2S_{\text{Co}} + 1) + \ln(2S_{\text{Fe}} + 1) \\ &\quad + \ln(2S_{\text{Nb}} + 1)] + S_n(\text{Co}) + S_n(\text{Nb}) + \delta S \\ &\approx 57.09 \text{ J K}^{-1} \text{ mol}^{-1}, \end{aligned} \quad (18)$$

$$\begin{aligned} S_{\text{Fe}_2\text{Nb}} &= S_0 + R[2 \ln(2S_{\text{Fe}} + 1) \\ &\quad + \ln(2S_{\text{Nb}} + 1)] + S_n(\text{Nb}) \\ &\approx 51.67 \text{ J K}^{-1} \text{ mol}^{-1}, \end{aligned} \quad (19)$$

where S_0 is the component derived from the basal (the same for all three compounds) lattice contribution to the specific heat, and $\delta S = \Delta S_{\text{mix}}(100 \text{ K}) \approx -4.25 \text{ J K}^{-1} \text{ mol}^{-1}$ is a correction accounting for the changes of the lattice contribution of the mixed compound. The corresponding estimates read

$$\Delta S_1 = S_{\text{Co}_2\text{Nb}} - S_{\text{Fe}_2\text{Nb}} \approx 19.34 \text{ J K}^{-1} \text{ mol}^{-1}, \quad (20)$$

$$\Delta S_2 = S_{\text{Co}_2\text{Nb}} - S_{\text{CoFeNb}} \approx 13.92 \text{ J K}^{-1} \text{ mol}^{-1}, \quad (21)$$

$$\Delta S_3 = S_{\text{CoFeNb}} - S_{\text{Fe}_2\text{Nb}} \approx 5.42 \text{ J K}^{-1} \text{ mol}^{-1}, \quad (22)$$

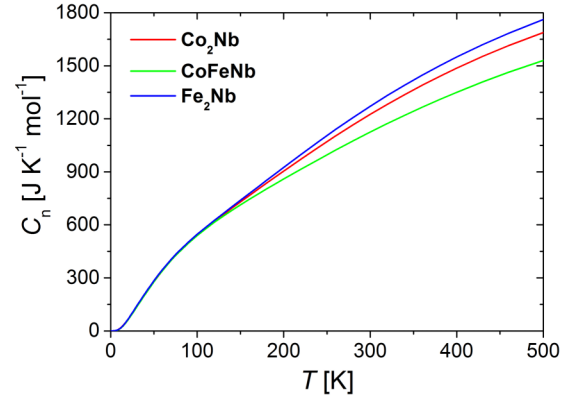


FIG. 12. The calculated normal heat capacities of the studied compounds.

and are depicted in Fig. 11 with dotted lines. They roughly agree with the observed values corroborating the assumed ionic spin content of the samples.

IV. MAGNETIC CONTRIBUTION TO HEAT CAPACITY

In general, the measured heat capacity is a conglomerate of several contributions stemming from various degrees of freedom. Except for the fortuitous case of a sharp transition phenomenon, the task to subdivide a total heat capacity among each contribution is far from straightforward. One of the most widely adopted approaches is to calculate the lattice heat capacity by adopting a plausible Debye temperature or a pair of Debye and/or Einstein temperatures [66–68]. A corresponding states method [69], a temperature derivative method [70], or a temperature-dependent Debye temperature method [71] count among other successful case-sensitive methods of separation. In the case under study, however, all these methods are not useful as the heat capacity anomalies due to magnetic interaction are extended over a wide temperature region. We therefore take an approach whose main principle is to calculate the lattice contribution based on a reasonable frequency spectrum, see Ref. [72] for detail. The measured heat capacities in the full temperature range were fitted using the following function:

$$C_p = C_{\text{normal}} + cT^{-2}, \quad (23)$$

where

$$C_{\text{normal}} = \text{Debye functions} + \text{Einstein functions} \quad (24)$$

is the sought-after lattice contribution to the heat capacity. The characteristic frequencies of the Einstein contributions were based on the known intramolecular vibrations for pyrazole [73], the water molecule [74], and the CN^- ligand [54], while the Debye cutoff frequencies were determined through the fit. The second term in Eq. (23) corresponds to the high-temperature contribution due to the magnetic short-range order. Table II lists the best fit parameters for the three studied compounds.

Using parameters in Table II, the normal (lattice) heat capacities were calculated, see Fig. 12. It is apparent that they almost perfectly overlap in the experimental window of $0.36\text{--}100 \text{ K}$. It is only $>110 \text{ K}$ that they start to diverge,

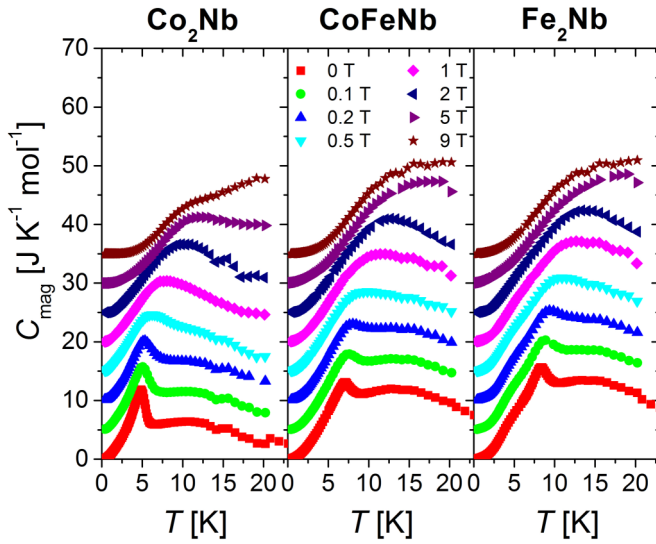


FIG. 13. Magnetic contributions to the heat capacity for the studied compounds. For the sake of clarity, the datasets corresponding to the nonzero field values have been shifted up successively by 5 units.

$d = 0.0116(2) \text{ J K mol}^{-1}$, $a = 1.57(9) \text{ J K mol}^{-1}$, $b = 2.09(3) \text{ K}$, $d = 0.0053(2) \text{ J K mol}^{-1}$, and $a = 1.41(9) \text{ J K mol}^{-1}$, $b = 2.03(3) \text{ K}$, $d = 0.0038(2) \text{ J K mol}^{-1}$ for Co_2Nb , CoFeNb , and Fe_2Nb , respectively. The total magnetic entropy involves four contributions: the first contribution ΔS_1 originates from the extrapolation of the magnetic heat capacity down to zero temperature; it is obtained by logarithmically integrating the first term in Eq. (25) with the best-fit parameter values in the range of 0–0.36 K; the second contribution ΔS_2 is calculated by numerically integrating the magnetic heat capacity in the range of 0.36 K– T_f , $\Delta S_2 = \int_{0.36}^{T_f} C_{\text{mag}}(T) d \ln T$; the third contribution ΔS_3 is due to the high-temperature magnetic heat capacity tail, it is obtained by logarithmically integrating the second term in Eq. (23) in the temperature range T_f – ∞ yielding $\Delta S_3 = cT_f^{-2}/2$; and finally, the last contribution ΔS_4 originates from the high-temperature tail of the nuclear contribution to the magnetic heat capacity given by the second term in Eq. (25); it is calculated by logarithmically integrating this term with the best-fit parameter value in the range of 0.36 K– ∞ , giving $\Delta S_4 = 3.85802d$, and should be subtracted from the total, leaving exclusively the contributions from the electronic degrees of freedom $\Delta S_{\text{mag}} = \Delta S_1 + \Delta S_2 + \Delta S_3 - \Delta S_4$. Table III collects the results of magnetic entropy calculations for the studied compounds.

TABLE III. The results of magnetic entropy calculations; $\Delta S_{\text{mag}} = \Delta S_1 + \Delta S_2 + \Delta S_3 - \Delta S_4$.

Entropy ($\text{J K}^{-1} \text{ mol}^{-1}$)	Co_2Nb	CoFeNb	Fe_2Nb
ΔS_1	0.0054	0.0074	0.0082
ΔS_2	16.8728	24.7126	26.8012
ΔS_3	0.1106	0.2850	0.2311
ΔS_4	0.0441	0.0203	0.0147
ΔS_{mag}	16.94	24.98	27.03
ΔS_{calc}	17.29	24.91	32.53

The last row in Table III shows the expected magnetic entropies due to the electronic degrees of freedom, calculated assuming the following spin states of the constitutive ions: $S_{\text{Co}} = \frac{1}{2}$, $S_{\text{Fe}} = 2$, and $S_{\text{Nb}} = \frac{1}{2}$. These values compare well with the experimental ones for Co_2Nb and CoFeNb , while for Fe_2Nb , the experimental value is largely underestimated. This may be attributed to a possible overestimation of the normal heat capacity in this case and/or to an effective attenuation of the spin of the Fe(II) ion due to a possible magnetocrystalline anisotropy. The latter would be consistent with the magnetization data at 2 K, cf. Fig. 6(b) in Ref. [54], where the theoretical mean-field curve (black solid line) obtained, assuming the high spin state of the Fe(II) ion, i.e., $S_{\text{Fe}} = 2$, systematically exceeds the experimental points (blue full circles). Indeed, ΔS_{calc} calculated with $S_{\text{Fe}} \approx \frac{3}{2}$ amounts to $28.82 \text{ J K}^{-1} \text{ mol}^{-1}$, which is closer to the experimental value of $27.03 \text{ J K}^{-1} \text{ mol}^{-1}$. Except for Fe_2Nb , the magnetic entropies inferred from the experimental data ΔS_{mag} exceed those calculated based on the presupposed spin content ΔS_{calc} . This is due to the assumption that the spin of the Co(II) ion is equal to $S_{\text{Co}} = \frac{1}{2}$, which corresponds to the ground Kramers doublet being exclusively populated. This is the case at sufficiently low temperatures; however, at higher temperatures, the excited Kramers doublets become more and more populated, enhancing the spin value toward the free-ion one $S_{\text{Co}} = \frac{3}{2}$.

A comment may be in order here. Let us note that the best fit values of the parameters in Eq. (25) are not randomly distributed but display a monotonous decrease from compound to compound, i.e., $a(b, d)_{\text{Co}_2\text{Nb}} > a(b, d)_{\text{CoFeNb}} > a(b, d)_{\text{Fe}_2\text{Nb}}$. That decrease of parameter d is consistent with the decrease of nuclear spin contributions observed for the studied compounds (twice the contribution from ^{59}Co plus once the contribution from ^{93}Nb for Co_2Nb , once the contribution from ^{59}Co plus once the contribution from ^{93}Nb for CoFeNb , and once the contribution from ^{93}Nb for Fe_2Nb). This tendency is consistently reflected in the correction entropy term ΔS_4 for which we have $\Delta S_4(\text{Co}_2\text{Nb}) > \Delta S_4(\text{CoFeNb}) > \Delta S_4(\text{Fe}_2\text{Nb})$. Similarly, the decreasing trend of parameter b , placed in the negative exponent, reflects the increasing trend in the electronic low-temperature spin content (twice spin $\frac{1}{2}$ of Co(II) plus once spin $\frac{1}{2}$ of Nb(IV) for Co_2Nb , once spin $\frac{1}{2}$ of Co(II) plus once spin 2 of Fe(II) plus once spin $\frac{1}{2}$ of Nb(IV) for CoFeNb , twice spin 2 of Fe(II) plus once spin $\frac{1}{2}$ of Nb(IV) for Fe_2Nb). It is more difficult to explain the decreasing trend of the multiplicative parameter a because of possible correlations with parameter b ; however, the increasing trend in the electronic spin content is consistently reflected in the low-temperature entropy contribution ΔS_1 for which we have $\Delta S_1(\text{Co}_2\text{Nb}) < \Delta S_1(\text{CoFeNb}) < \Delta S_1(\text{Fe}_2\text{Nb})$. The best fit values of parameter c in Eq. (23) $c_{\text{Co}_2\text{Nb}} < c_{\text{CoFeNb}} < c_{\text{Fe}_2\text{Nb}}$ reflect likewise the increasing trend in the electronic spin content. Correction ΔS_3 , for which we have $\Delta S_3(\text{Co}_2\text{Nb}) < \Delta S_3(\text{CoFeNb}) > \Delta S_3(\text{Fe}_2\text{Nb})$, displays admittedly a different trend, but it correctly reflects the expected attenuation of the short-range order in the mixed compound. In conclusion, the reported procedure amply deserves to be deemed reliable and convincing.

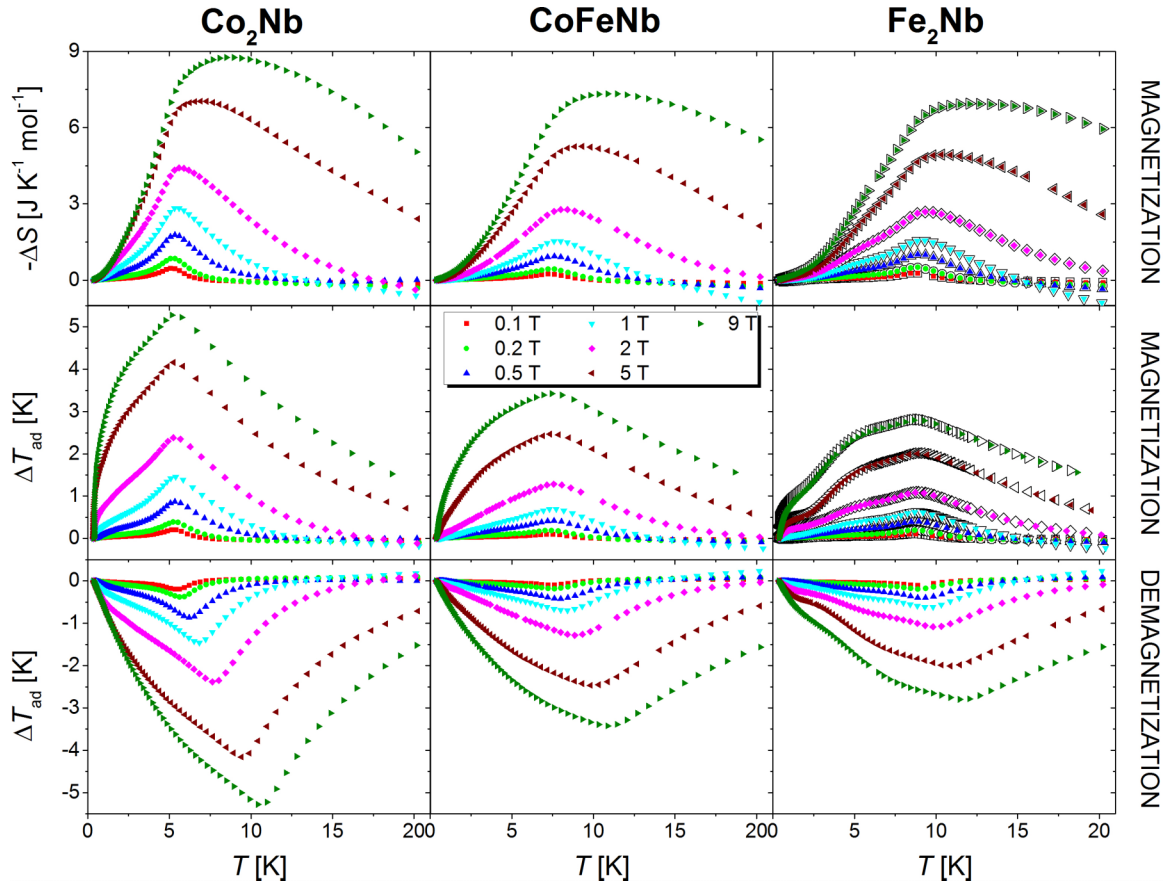


FIG. 14. Temperature dependence of the isothermal entropy change ΔS_M in the magnetization direction (upper panel), the adiabatic temperature change ΔT_{ad} in the magnetization direction (middle panel), and the adiabatic temperature change ΔT_{ad} in the demagnetization direction (lower panel) for an indicated array of magnetic field change values. Black open symbols in the panels displaying ΔS_M and ΔT_{ad} in the magnetization direction for Fe_2Nb show the data obtained independently and published in Ref. [58]; the agreement is close to perfect.

V. MCE

A. Isothermal entropy change ΔS_M and adiabatic temperature change ΔT_{ad}

The two main MCE characteristics of the studied compound, i.e., the temperature dependence of the isothermal entropy change ΔS_M and the adiabatic temperature change ΔT_{ad} , were determined indirectly using the measured heat capacity values. Here, ΔS_M was calculated using the following formula:

$$\begin{aligned} \Delta S_M(T, \Delta H = 0 \rightarrow H) & \\ & \equiv \Delta S_M(T, H) \\ & = \int_{T_{\min}}^T \frac{C_p(T', H) - C_p(T', H = 0)}{T'} dT', \quad (26) \end{aligned}$$

where T_{\min} denotes the left boundary of the experimental window. In this way, we deliberately neglect the entropy contribution in the interval $(0, T_{\min})$, which involves both the nuclear contribution as well as the contribution from electronic degrees of freedom. While the former contribution is difficult to follow, especially in nonzero magnetic field, the uncertainty associated with the latter one is on the order of the contribution ΔS_1 in Table III. The electronic contribution to the specific heat is associated with the localized electrons

residing on the outermost shells of the Co(II) and Fe(II) ions; thus, it is magnetic in character (the studied compounds are isolators, so no contribution from the itinerant electrons is present). The adiabatic temperature change ΔT_{ad} was estimated based on the following formula:

$$\Delta T_{ad}(H_i \rightarrow H_f) = [T(S, H_f) - T(S, H_i)]_S, \quad (27)$$

which requires the inversion of the temperature dependence of the total entropy $S(T, H)$ calculated similarly with the lower cutoff temperature T_{\min} . While ΔS_M was calculated in the magnetization direction, where the magnetic field change consists of switching on the field $H_i = 0 \rightarrow H_f = H$, ΔT_{ad} was calculated additionally in the demagnetization direction involving switching off of the field, i.e., $H_i = H \rightarrow H_f = 0$. Figure 14 collects the corresponding results.

It is apparent from Fig. 14 that, while the amplitudes of both quantities increase with increasing field change values, they show a decreasing trend when looking from compound Co_2Nb through CoFeNb to Fe_2Nb . The former behavior may be attributed to the effect of quenching the magnetic entropy by the application of the magnetic field, i.e., the stronger the field, the larger the quench. To understand the latter effect, let us note that the signals of $|\Delta S_M|$ and $|\Delta T_{ad}|$ are consistently centered around the corresponding phase transition

TABLE IV. Peak values of quantities ΔS_M and ΔT_{ad} .

$\mu_0\Delta H$ (T)	Magnetization			Demagnetization		
	T_{max} (K)	$ \Delta S_M ^{max}$ ($\text{J K}^{-1} \text{mol}^{-1}$)	T_{max} (K)	ΔT_{ad}^{max} (K)	T_{max} (K)	$ \Delta T_{ad} ^{max}$ (K)
Co ₂ Nb [$T_c = 4.87(8)$ K]						
0.1	5.08	0.46	5.42	0.20	5.62	0.20
0.2	5.34	0.85	5.24	0.39	5.62	0.39
0.5	5.33	1.78	5.34	0.87	6.21	0.87
1	5.60	2.83	5.39	1.46	6.85	1.46
2	5.59	4.41	5.25	2.38	7.63	2.38
5	6.91	7.04	5.25	4.16	9.41	4.16
9	8.94	8.75	5.15	5.28	10.43	5.28
CoFeNb [$T_c = 7.1(2)$ K]						
0.1	7.23	0.23	7.52	0.10	7.62	0.10
0.2	7.22	0.43	7.43	0.19	7.62	0.19
0.5	7.61	0.94	7.59	0.42	8.01	0.42
1	7.99	1.53	7.72	0.69	8.41	0.69
2	7.99	2.77	7.57	1.28	8.86	1.28
5	9.32	5.26	7.34	2.47	9.81	2.47
9	10.88	7.33	7.45	3.42	10.88	3.42
Fe ₂ Nb [$T_c = 8.44(3)$ K]						
0.1	8.89	0.27	8.78	0.11	8.89	0.11
0.2	8.89	0.50	8.70	0.19	8.89	0.19
0.5	8.88	1.02	8.95	0.40	9.35	0.40
1	9.32	1.56	8.70	0.62	9.32	0.62
2	9.32	2.69	8.73	1.08	9.81	1.08
5	10.33	4.93	8.86	2.01	10.87	2.01
9	12.05	6.94	8.65	2.80	11.45	2.80

temperatures which shift rightward from sample to sample. In addition, Fig. 13 implies that the thermal effects $\Delta Q(H) = \int C_{mag}(H)dT$ associated with the three samples are comparable. Then the entropic effect $\Delta S(T, H) \propto \Delta Q(H)/T$ becomes roughly inversely proportional to temperature, i.e., the higher the temperature, the smaller the entropy changes. Table IV collects the peak values of the quantities ΔS_M and ΔT_{ad} for the three compounds.

Table IV shows that the peak temperatures T_{max} are all placed above the transition temperature points T_c . For the isothermal entropy change $|\Delta S_M|$ as well as the adiabatic temperature change $|\Delta T_{ad}|$ in the demagnetization mode, the peak temperatures shift visibly toward higher temperatures with the increasing field change values. In the case of ΔT_{ad} in the magnetization mode, no clear trend in the dependence of T_{max} on $\mu_0\Delta H$ can be observed, with the peak temperatures being stiffly anchored slightly above T_c . The values of $|\Delta S_M|^{max}$ detected for $\mu_0\Delta H = 5$ T amount to 7.04, 5.26, and 4.93 $\text{J K}^{-1} \text{mol}^{-1}$ for Co₂Nb, CoFeNb, and Fe₂Nb, respectively, and are on the order of those obtained for the same field change in the isostructural compounds $\{[M^{II}(\text{pyrazole})_4]_2[\text{Nb}^{IV}(\text{CN})_8] \cdot 4\text{H}_2\text{O}\}_n$ with $M = \text{Mn}$ (6.83 $\text{J K}^{-1} \text{mol}^{-1}$, $T_c = 22.8$ K) and $M = \text{Ni}$ (6.1 $\text{J K}^{-1} \text{mol}^{-1}$, $T_c = 13.4$ K) [50,51]. Although the spin value of the Ni(II) center ($S_{Ni} = 1$) is lower than that of the Fe(II) ion ($S_{Fe} = 2$), the compound with $M = \text{Ni}$ shows larger MCE effect. This may be due to both the local anisotropy of the Fe(II) center, which is known to affect adversely the MCE effect [42], as well as the fact that the exchange coupling in the compound containing Ni(II) is of ferro-

magnetic character [54]. A similar difference occurs for the compounds with $M = \text{Co}$ and Mn , where the effective spin of the Co(II) ion in the low-temperature regime is as low as $S_{Co} = \frac{1}{2}$, while the spin of the Mn(II) ion is $S_{Mn} = \frac{5}{2}$, yet we observe a larger $|\Delta S_M|^{max}$ for the first sample than for the other. This may be understood by remembering that the Mn compound orders at considerably larger temperature (~ 4.7 times) than the Co₂Nb, and the entropic effect is roughly inversely proportional to temperature, as discussed above. The values of ΔT_{ad} detected for $\mu_0\Delta H = 5$ T amount to 4.16, 2.47, and 2.01 $\text{J K}^{-1} \text{mol}^{-1}$ for Co₂Nb, CoFeNb, and Fe₂Nb, respectively, and are larger or comparable with those observed for the same field change for the isostructural compounds $\{[M^{II}(\text{pyrazole})_4]_2[\text{Nb}^{IV}(\text{CN})_8] \cdot 4\text{H}_2\text{O}\}_n$ with $M = \text{Mn}$ (1.42 K) and $M = \text{Ni}$ (2.0 K) [50,51]. They also exceed those found for Mn₂-pyridazine-[Nb(CN)₈] (1.5 K for $\mu_0\Delta H = 5$ T) [52] and hexacyanochromate Prussian blue analogues (1.2 K for $\mu_0\Delta H = 7$ T) [47].

It is interesting to look at MCE for the lowest field change values $\mu_0\Delta H = 0.1, 0.2, 0.5,$ and 1 T, see Fig. 14. In these cases, the inverse MCE (heating under adiabatic demagnetization) is present above the transition temperature for the three compounds. The effect increases with increasing field change value to diminish or completely vanish for $\mu_0\Delta H \geq 2$ T. A similar effect was observed for the Mn analogue [51]. A possible explanation could be that the low field cannot reorient the correlated clusters above the transition temperature, and the only effect it can cause is the local flipping of the magnetic moments, which can be seen as a disordering factor. Thus, there is an additional contribution to the in-field entropy so

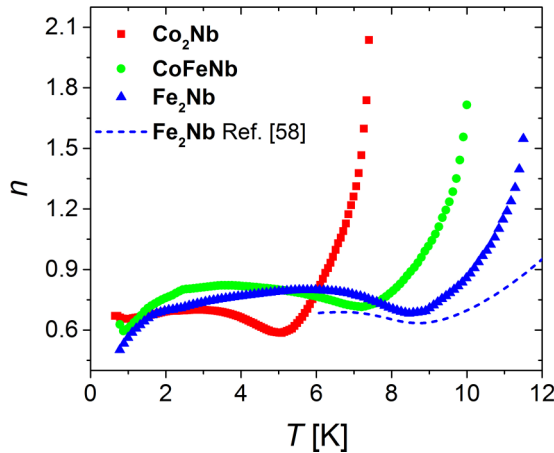


FIG. 15. Temperature dependence of exponent n quantifying the field dependence of the isothermal entropy change ΔS_M for the three studied compounds.

that the entropy in zero field is slightly smaller than that in a nonzero field.

B. Field dependence of MCE

The field dependence of MCE has been studied intensively, either experimentally [45,51,75,76] or from a theoretical viewpoint by using the description within the mean-field model [77] or employing the equation of state of materials with the second-order magnetic phase transition [78,79]. The parameter conveniently quantifying the local sensitivity of the isothermal entropy change to the external field amplitude $H = \Delta H = H_f - H_i (= 0)$ is exponent n defined by the following derivative:

$$n = \frac{d \ln |\Delta S_M|}{d \ln H}. \quad (28)$$

The value of n means that, in the vicinity of a given thermodynamic point (T, H) , the entropy change behaves approximately as H^n . The high-temperature limit of an n vs T curve, $n = 2$, is the consequence of the Curie-Weiss law, where the magnetic entropy change using the following equation:

$$\Delta S_M(T, \Delta H = H_f - H_i) = \int_{H_i}^{H_f} \frac{\partial M(T, H)}{\partial T} dH \quad (29)$$

implied by the Maxwell relation, yields a quadratic field dependence of ΔS_M . The value of n in the low-temperature regime cannot be easily predicted; however, if the magnetization displays only a weak field dependence there, Eq. (29) implies $n = 1$. The temperature dependence of the field-averaged value of exponent n for the compounds under study, estimated based on the entropy data in Fig. 14, is shown in Fig. 15. Parameter n displays a smooth decrease on cooling from the values ~ 2 , in agreement with what might be expected. Next, it attains the minimum of 0.59, 0.71, and 0.68 at 5.08, 7.21, and 8.47 K, i.e., slightly above the transition temperature, for Co_2Nb , CoFeNb , and Fe_2Nb , respectively. In the low-temperature regime, exponent n assumes again a decreasing trend, displaying the second minimum at the lowest temperatures but for compound Fe_2Nb . The value of exponent

TABLE V. Temperatures T_C and T_H . The values marked by an asterisk correspond to the endpoint entropy data placed above the half-maximum level.

$\mu_0 \Delta H$ (T)	Co_2Nb		CoFeNb		Fe_2Nb	
	T_C (K)	T_H (K)	T_C (K)	T_H (K)	T_C (K)	T_H (K)
0.1	4.11	5.97	5.57	8.55	7.02	10.01
0.2	4.00	6.30	5.30	8.91	6.83	10.37
0.5	3.88	7.20	5.20	9.91	6.35	11.33
1	3.69	8.28	5.08	10.84	5.84	12.21
2	3.52	10.29	5.01	13.27	5.63	14.85
5	3.62	17.17	4.98	18.77	5.71	20.18*
9	3.89	20.16*	5.16	20.23*	5.79	20.21*

n at the transition temperature T_C has been demonstrated to be related to the critical exponents of a material [79]:

$$n|_{T_C} = 1 + \frac{\beta - 1}{\beta + \gamma}. \quad (30)$$

The values of n at T_C practically coincide with its values at the minima being equal to 0.59, 0.72, and 0.68 for Co_2Nb , CoFeNb , and Fe_2Nb , respectively. They are close to the value of 0.6424(4) obtained with Eq. (30) and the theoretical estimates for the 3D Heisenberg universality class [80], namely, $\beta = 0.3689(3)$ and $\gamma = 1.3960(9)$.

The dashed line in Fig. 15 shows the temperature dependence of exponent n obtained previously and published in Ref. [58] for Fe_2Nb . The corresponding values are lower than those found here (blue triangles). This is due to the difference in the method of calculation employed. In Ref. [58], the exponent was found as the slope of the linear function fitted to the experimental points $[\ln H_i, \ln |\Delta S_M(H_i, T)|]$, where $H_i \in \{0.1, 0.2, 0.5, 1, 2, 5, 9\}$ T. However, a detailed analysis revealed that the corresponding points frequently deviate from the straight line, and consequently, the parameter n becomes field dependent. We therefore decided to calculate the slope locally, i.e., $n_i = \frac{\ln |\Delta S_M(H_{i+1}, T)| / \Delta S_M(H_i, T)}{\ln(H_{i+1}/H_i)}$, and take the average $\bar{n} = \frac{1}{7} \sum_{i=1}^7 n_i$ to represent the final value of the exponent.

C. RC

A commonly accepted measure for the performance of a substance undergoing a magnetic cooling cycle is the RC, defined as [81,82]

$$\text{RC} = \int_{T_C}^{T_H} \Delta S_M(T, \Delta H) dT, \quad (31)$$

where the temperatures T_C and T_H of the cold and hot reservoir, respectively, are usually selected to cover the full width at half maximum of the entropy change peak $\Delta S_M(T, \Delta H)$. This quantity is a measure of how much heat can be transferred between the cold and hot reservoirs in one ideal refrigeration cycle. Table V collects the values of T_C and T_H determined in the above way for all field change values and all the studied compounds.

In Fig. 16, the field dependence of RC is shown for the three studied samples. As might be expected, RC is an increasing function of the field change value. For CoFeNb and

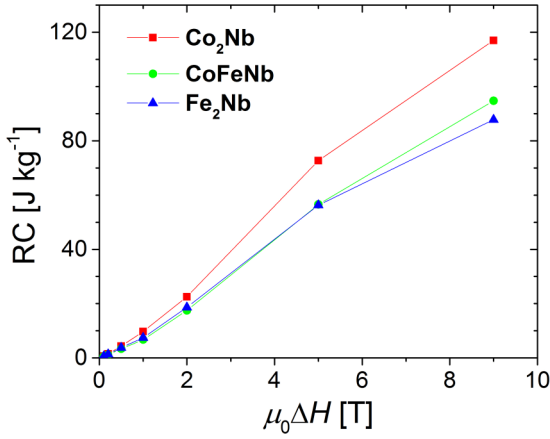


FIG. 16. Field dependence of the refrigerant capacity for the studied samples.

Fe_2Nb , the RC curves almost coincide, while for Co_2Nb , the RC values exceed those calculated for the remaining compounds. RC for the field change of $\mu_0\Delta H = 5 \text{ T}$ amounts to 72.7, 56.5, and 56.3 J kg^{-1} for Co_2Nb , CoFeNb , and Fe_2Nb , respectively. These values are placed below those found for the same field change for the Mn (132.9 J kg^{-1}) and Ni (73.1 J kg^{-1}) analogues [50].

D. The Ericsson cycle

Among the thermodynamic cycles, important for magnetic refrigeration, the regeneration Ericsson cycle is especially worth mentioning [83,84]. Let us consider two regeneration Ericsson cycles, referred to in what follows as Ericsson 1 and Ericsson 2 and depicted in the (T, S) plane of Fig. 17 in blue and red, respectively. Cycle Ericsson 1 ($A \rightarrow B \rightarrow D \rightarrow E \rightarrow A$) consists of two isothermal processes ($A \rightarrow B$ at temperature T_H and $D \rightarrow E$ at temperature T_C) and two isofield processes ($B \rightarrow D$ at applied field H and $E \rightarrow A$ at zero applied field). Similarly, cycle Ericsson 2 ($F \rightarrow C \rightarrow D \rightarrow E \rightarrow F$) consists of two isothermal processes ($F \rightarrow C$ at temperature T_{\max} and $D \rightarrow E$ at temperature T_C) and two isofield processes ($C \rightarrow D$ at applied field H and $E \rightarrow F$ at zero applied field). Temperatures T_C and T_H of the cold and hot reservoirs correspond to the endpoints of the full width at half maximum of the entropy change peak $|\Delta S_M(T, H)|$, see Table V, while T_{\max} is the peak temperature of $\Delta S_M(T, H)$, see the second column in Table IV.

Let us first analyze cycle Ericsson 1. For this cycle, the heat Q_C absorbed during the isothermal process $D \rightarrow E$ and the heat Q_H rejected at the isothermal process $A \rightarrow B$ can be calculated by

$$\begin{aligned} Q_C &= \int_{D \rightarrow E} T dS = -T_C \Delta S_M(T_C, H) > 0, \\ Q_H &= \int_{A \rightarrow B} T dS = T_H \Delta S_M(T_H, H) < 0, \end{aligned} \quad (32)$$

where the isothermal entropy change $\Delta S_M(T, H)$ is given in Eq. (26). In the present case, where $T_C < T_{\max} < T_H$, the

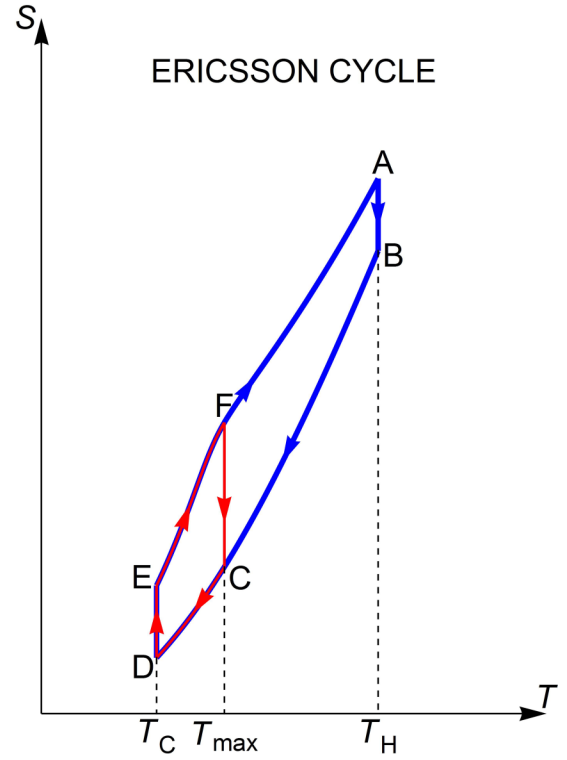


FIG. 17. The regeneration Ericsson cycles operating between T_C and T_H (Ericsson 1, blue) and T_C and T_{\max} (Ericsson 2, red). The genuine entropy data in $\mu_0 H = 0$ and 2 T for Co_2Nb have been used.

nonperfect regeneration heat quantity ΔQ must be divided in two parts $\Delta Q = -(Q_{EA} + Q_{BD}) = \Delta Q^+ + \Delta Q^-$, where

$$\Delta Q^- = \int_{T_C}^{T_{\max}} T \frac{\partial \Delta S_M(T, H)}{\partial T} dT < 0 \quad (33)$$

quantifies the heat that must be compensated by the hot reservoir, and

$$\Delta Q^+ = \int_{T_{\max}}^{T_H} T \frac{\partial \Delta S_M(T, H)}{\partial T} dT > 0 \quad (34)$$

quantifies the heat that must be released to the cold reservoir; otherwise, the temperature of the regenerator will be changed, and the cycle would not operate properly. Here, ΔQ^+ corresponds to the situation where the heat transferred from the working substance to the regenerator is larger than that transferred from the regenerator to the working substance. In the case of ΔQ^- , just the reverse holds, i.e., the heat transferred from the working substance to the regenerator is smaller than that transferred from the regenerator to the working substance. In this way, the net cooling quantity Q_L is reduced as compared with Q_C , i.e., $Q_L = Q_C - \Delta Q^+$. According to the first law of thermodynamics, the work input of the refrigeration cycle W is given by the following formula:

$$\begin{aligned} W &= -(Q_C + Q_H - \Delta Q) \\ &= T_C \Delta S_M(T_C, H) \\ &\quad - T_H \Delta S_M(T_H, H) + \int_{T_C}^{T_H} T \frac{\partial \Delta S_M(T, H)}{\partial T} dT. \end{aligned} \quad (35)$$

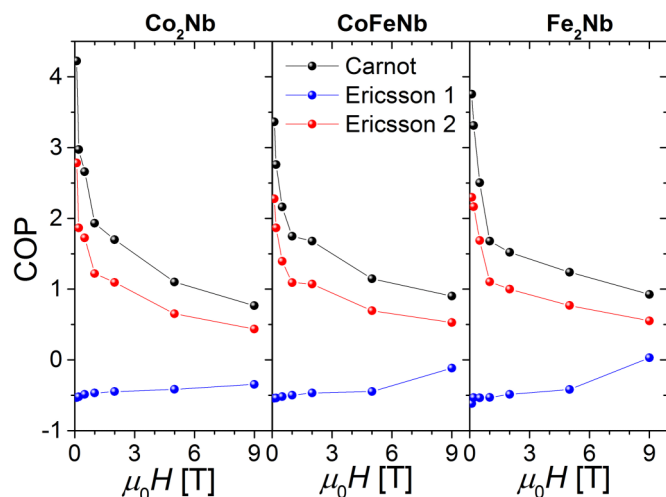


FIG. 18. Field dependence of the coefficient of performance of three indicated thermodynamic cycles for the studied compounds.

Finally, the coefficient of performance (COP) of the refrigeration cycle is given by

$$\text{COP} = \frac{Q_L}{W}. \quad (36)$$

The discussion of cycle Ericsson 2 would be fully analogous. It is sufficient to consider that $T_H = T_{\max}$ in this case. Immediately, Eq. (34) implies that quantity ΔQ^+ vanishes, and consequently, the net cooling quantity $Q_L = Q_C$ is not reduced. One therefore should expect enhanced COP values. The COP values for the Ericsson cycles should be compared with that of the Carnot cycle operating between the same temperatures T_C and T_H of the cold and hot reservoirs. The main difference is that the isofield processes of the Ericsson cycle are replaced by the adiabatic ones. This is formally equivalent to the situation where the $\Delta S_M(T, H)$ curve is flat between T_C and T_H , i.e., then $\partial \Delta S_M(T, H) / \partial T = 0$ and Eqs. (32)–(36) imply that

$$\text{COP}_{\text{Carnot}} = \frac{T_C}{T_H - T_C}. \quad (37)$$

Figure 18 shows the field dependence of the COP of cycles Ericsson 1, Ericsson 2, and the Carnot cycle operating between temperatures T_C and T_H for the studied compounds. COPs for all three samples display a similar pattern. Quite surprisingly, COP of Ericsson 1 assumes systematically negative values except for that for Fe₂Nb at $\mu_0 H = 9$ T, where it turns slightly positive. This implies that this refrigeration cycle, operating in the full width of half maximum of $|\Delta S_M(T, H)|$, becomes totally ineffective, although it improves steadily with increasing magnetic field. Shifting the temperature of the hot reservoir T_H down to T_{\max} , which is the case for Ericsson 2, remedies the situation, and the corresponding COP is positive and lower than that of the Carnot cycle. However, it shows a decreasing trend with increasing magnetic field. At the same time, the RC was demonstrated to be an increasing function of the field change $\mu_0 \Delta H$, see Fig. 16, assuming very small values for the lowest field change values. In view of these facts, a compromise must be made for the Ericsson 2 cycle to be most efficient. A possible candidate quantifying

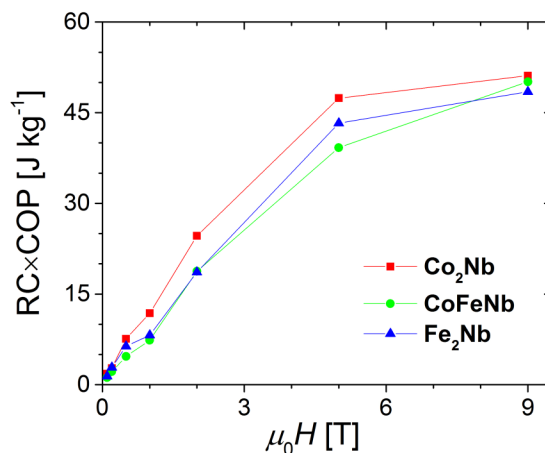


FIG. 19. Field dependence of product refrigeration capacity (RC) × coefficient of performance (COP) quantifying the efficiency of cycle Ericsson 2 for the studied compounds.

its efficiency is the product $\text{RC} \times \text{COP}$, whose largest value should roughly indicate the most efficient cycle. Figure 19 shows the field dependence of the $\text{RC} \times \text{COP}$ product for the three studied compounds. It implies that the Ericsson 2 cycle should be most efficient for the maximal studied value of the applied field ($=9$ T) with irrelevant differences between the compounds. At the same time, the Ericsson 2 cycle using Fe₂Nb as the working substance at 9 T would be less efficient than that using Co₂Nb at the lower field value of 5 T.

VI. CONCLUSIONS

We have reported a comprehensive study of thermodynamic properties of three samples of bimetallic molecular magnets $[\text{Co}^{\text{II}}(\text{pyrazole})_4]_{2x}[\text{Fe}^{\text{II}}(\text{pyrazole})_4]_{2(1-x)}[\text{Nb}^{\text{IV}}(\text{CN})_8] \cdot 4\text{H}_2\text{O}$ with $x = 0, 0.5$, and 1, where the middle compound represents a substitutional mixture of the two marginal ones. The three samples display the same crystallographic structure. Their heat capacities were measured in the temperature range 0.36–100 K without applied field as well as in the field of $\mu_0 H = 0.1, 0.2, 0.5, 1, 2, 5$, and 9 T. The results revealed anomalies assigned to the second-order phase transitions to magnetically ordered phases with the transition temperatures estimated to amount to 4.87(8), 7.1(2), and 8.44(3) K for $x = 1, 0.5$, and 0, respectively. The heat capacity results were analyzed to discuss the stability of the mixed compound and the MCE. The Gibbs energy of mixing turned out to be positive but smaller in magnitude than the energy of thermal fluctuations, which implies that the mixed sample is most probably metastable in the full detected temperature range. The negative values of the enthalpy of mixing are explained in terms of favoring a direct neighborhood of the Co and Fe ions in the solid solution CoFeNb. The negative values of the entropy of mixing can be rationalized by supposing that the lattice of the solid solution sample becomes more rigid due to the requirement of accommodating two different atoms within the same lattice structure. To extract the magnetic contribution to the heat capacity, we took an approach whose main principle is to calculate the lattice contribution based

on a reasonable frequency spectrum. While C_{mag} is consistent with the expected spin content of the Co(II) and Nb(IV) ions ($S_{\text{Co}} = \frac{1}{2}$, $S_{\text{Nb}} = \frac{1}{2}$), it suggests an effective attenuation of the spin of the Fe(II) ion ($S_{\text{Fe}} = 2$) due to a possible magnetocrystalline anisotropy. Taking advantage of the in-field heat capacity measurements, the MCE was described in terms of the isothermal entropy change ΔS_{M} and the adiabatic temperature change ΔT_{ad} . The magnitudes of these quantities turned out to be typical for the class of molecular magnets. The analysis of the field dependence of ΔS_{M} implied that the studied compounds belong to the universality class of the 3D Heisenberg model. To get some practical insight into the issue of magnetic refrigeration, the regeneration Ericsson cycles employing the studied compounds as the working substance were considered. Most surprisingly, the Ericsson cycle operating between the temperatures corresponding to the full width at half maximum of the $|\Delta S_{\text{M}}|$ signal turned out to be completely ineffective. It was only by shifting the temperature of the hot reservoir T_{H} down to the temperature T_{max} corresponding to $|\Delta S_{\text{M}}|^{\text{max}}$ that the COP became positive and comparable with that of the Carnot cycle. To determine the optimal value of the magnetic field for which the Ericsson cycle is most efficient, the product of the RC and the COP was employed. The calculations indicated that the regeneration Ericsson cycle operating between T_{C} and T_{max} should be most efficient for the maximal studied value of the applied field ($=9$ T) with irrelevant differences between the compounds. The above findings place the studied samples among possible candidates for cryogenic refrigeration.

APPENDIX: THE MOLECULAR FIELD MODEL FOR AN EXCHANGE COUPLED SYSTEM WITH PARTIAL SUBSTITUTION

Let us assume that the system consists of two sublattices A and B with stoichiometric factors ν_{A} and ν_{B} , respectively. Sublattice B is occupied by the B-type ions with spin S_{B} and the Landé factor g_{B} , while sites of sublattice A are randomly filled with the A_1 -type ions (S_{A_1} , g_{A_1}) and the A_2 -type ions (S_{A_2} , g_{A_2}) with x denoting the number concentration of the latter. Thus, the system may be described by the formula $(\text{A}_{1-x}\text{A}_2x)_{\mu_{\text{A}}}\text{B}_{\mu_{\text{B}}}$. The Hamiltonian pertinent to the system is given by the following formula:

$$\hat{H} - J_{\text{A}_1\text{B}} \sum_{(ij)} \hat{S}_{\text{A}_1i} \cdot \hat{S}_{\text{B}j} - J_{\text{A}_2\text{B}} \sum_{(ij)} \hat{S}_{\text{A}_2i} \cdot \hat{S}_{\text{B}j} + \mu_{\text{B}} \sum_i (g_{\text{A}_1} \hat{S}_{\text{A}_1i} + g_{\text{A}_2} \hat{S}_{\text{A}_2i} + g_{\text{B}} \hat{S}_{\text{B}i}) \cdot \vec{H}, \quad (\text{A1})$$

where (ij) denotes the summation over the pairs of the nearest neighbors, J_{XY} is the superexchange coupling constant between the X - and Y -type ions, μ_{B} is the Bohr magneton, and \vec{H} is the external magnetic field. We neglect the superexchange coupling within the A sublattice ($J_{\text{AA}} = 0$) and the B sublattice

($J_{\text{BB}} = 0$) as, in the case under study, the corresponding bridges involve many atoms. A full solution of the model is an extremely complex task that could only be tackled by the quantum Monte Carlo methods. We therefore decide here for a simplified approach based on the molecular field approximation (MFA). In the framework of MFA, the Hamiltonian in Eq. (A1) is reduced to the following form:

$$\hat{H} = g_{\text{A}_1} \mu_{\text{B}} \hat{S}_{\text{A}_1} \cdot \vec{H}_{\text{A}_1} + g_{\text{A}_2} \mu_{\text{B}} \hat{S}_{\text{A}_2} \cdot \vec{H}_{\text{A}_2} + g_{\text{B}} \mu_{\text{B}} \hat{S}_{\text{B}} \cdot \vec{H}_{\text{B}}, \quad (\text{A2})$$

where the molecular fields \vec{H}_X ($X = \text{A}_1, \text{A}_2, \text{B}$) read

$$\begin{aligned} \vec{H}_{\text{A}_1} &= \vec{H} + \Lambda_{\text{A}_1\text{B}} \vec{M}_{\text{B}}, \\ \vec{H}_{\text{A}_2} &= \vec{H} + \Lambda_{\text{A}_2\text{B}} \vec{M}_{\text{B}}, \\ \vec{H}_{\text{B}} &= \vec{H} + \Lambda_{\text{BA}_1} \vec{M}_{\text{A}_1} + \Lambda_{\text{BA}_2} \vec{M}_{\text{A}_2}. \end{aligned} \quad (\text{A3})$$

Quantity \vec{M}_X denotes the molar magnetization of sublattice X , and the molecular field constants Λ_{XY} read

$$\begin{aligned} \Lambda_{\text{A}_1\text{B}} &= \frac{J_{\text{A}_1\text{B}} Z_{\text{A}_1\text{B}}}{N_{\text{A}} \mu_{\text{B}}^2 \nu_{\text{B}} g_{\text{A}_1} g_{\text{B}}}, & \Lambda_{\text{BA}_1} &= \frac{J_{\text{A}_1\text{B}} Z_{\text{BA}_1}}{N_{\text{A}} \mu_{\text{B}}^2 \nu_{\text{A}} (1-x) g_{\text{A}_1} g_{\text{B}}}, \\ \Lambda_{\text{A}_2\text{B}} &= \frac{J_{\text{A}_2\text{B}} Z_{\text{A}_2\text{B}}}{N_{\text{A}} \mu_{\text{B}}^2 \nu_{\text{B}} g_{\text{A}_2} g_{\text{B}}}, & \Lambda_{\text{BA}_2} &= \frac{J_{\text{A}_2\text{B}} Z_{\text{BA}_2}}{N_{\text{A}} \mu_{\text{B}}^2 \nu_{\text{A}} x g_{\text{A}_2} g_{\text{B}}}, \end{aligned} \quad (\text{A4})$$

where Z_{XY} denotes the number of the nearest neighbor Y -type ions of the X -type ion. It is clear that $Z_{\text{A}_1\text{B}} = Z_{\text{A}_2\text{B}} = Z_{\text{AB}}$, $Z_{\text{BA}_1} = (1-x)Z_{\text{BA}}$, and $Z_{\text{BA}_2} = xZ_{\text{BA}}$. Moreover, the number of the coupling connections between the A- and B-type ions in a mole of the compound may be written either as $N_{\text{A}} \nu_{\text{A}} Z_{\text{AB}}$ or as $N_{\text{A}} \nu_{\text{B}} Z_{\text{BA}}$; hence, $\nu_{\text{A}} Z_{\text{AB}} = \nu_{\text{B}} Z_{\text{BA}}$. The above relations and Eq. (A4) imply that $\Lambda_{\text{A}_1\text{B}} = \Lambda_{\text{BA}_1} \equiv \Lambda_1$ and $\Lambda_{\text{A}_2\text{B}} = \Lambda_{\text{BA}_2} \equiv \Lambda_2$; thus, there only two independent molecular field constants in the model. For an arbitrary thermodynamic point (T, H) , the molecular field model defined in Eqs. (A2)–(A4) should be solved by an iterative numerical method. However, in the special case where the temperature is high compared with $\max(J_{\text{A}_1\text{B}}/k_{\text{B}}, J_{\text{A}_2\text{B}}/k_{\text{B}})$ (k_{B} is the Boltzmann constant), one can venture to calculate the magnetic susceptibility χ of the system. An additional simplification stems from the fact that the model is isotropic (all exchange interactions are of the isotropic Heisenberg type), and the scalar counterpart of Eq. (A3) can be used. Then the system is in the paramagnetic state, and the molar magnetizations are directly proportional to the magnetic field, i.e., $M_X = \chi_X H_X$, where

$$\chi_X = \frac{N_{\text{A}} \mu_{\text{B}}^2 \nu_X c_X g_X^2 S_X (S_X + 1)}{3k_{\text{B}} T} \quad (\text{A5})$$

is the paramagnetic molar susceptibility of sublattice X , and c_X is the number concentration of the X -type ions ($c_{\text{A}_1} = 1-x$, $c_{\text{A}_2} = x$, and $c_{\text{B}} = 1$). The system of linear equations $M_X = \chi_X H_X$ ($X = \text{A}_1, \text{A}_2, \text{B}$) can be solved by the Cramer method for M_X , and the total susceptibility of the system can be calculated as $\chi = (M_{\text{A}_1} + M_{\text{A}_2} + M_{\text{B}})/H$:

$$\chi = \frac{\chi_{\text{A}_1} + \chi_{\text{A}_2} + \chi_{\text{B}} + 2\chi_{\text{A}_1}\chi_{\text{B}}\Lambda_1 + 2\chi_{\text{A}_2}\chi_{\text{B}}\Lambda_2 - \chi_{\text{A}_1}\chi_{\text{A}_2}\chi_{\text{B}}(\Lambda_1 - \Lambda_2)^2}{1 - \chi_{\text{A}_1}\chi_{\text{B}}\Lambda_1^2 - \chi_{\text{A}_2}\chi_{\text{B}}\Lambda_2^2}. \quad (\text{A6})$$

The MFA estimate of the transition temperature T_c may be found through the straightforward algebra by solving the equation $\chi^{-1} = 0$ for T . The x -dependent result may be written

$$T_c(x) = \sqrt{(1-x)[T_c(0)]^2 + x[T_c(1)]^2}, \quad (\text{A7})$$

where the extreme transition temperatures read

$$T_c(0) = \frac{N_A \mu_B^2 g_{A_1} g_B}{3k_B} \Lambda_1 \sqrt{\nu_A \nu_B S_{A_1} (S_{A_1} + 1) S_B (S_B + 1)},$$

$$T_c(1) = \frac{N_A \mu_B^2 g_{A_2} g_B}{3k_B} \Lambda_2 \sqrt{\nu_A \nu_B S_{A_2} (S_{A_2} + 1) S_B (S_B + 1)}. \quad (\text{A8})$$

In the case under study, sublattice A corresponds to the Co sublattice in Co_2Nb ; next, it is substituted by the Fe ions, so that $A_1 = \text{Co}$ and $A_2 = \text{Fe}$. The B sublattice corresponds to the untouched Nb ions, i.e., $B = \text{Nb}$. The pertinent values of parameters are $\nu_{\text{Co}} = 2$, $\nu_{\text{Nb}} = 1$, $Z_{\text{NbCo}} = 4$, $Z_{\text{CoNb}} = 2$, $S_{\text{Co}} = \frac{1}{2}$, $S_{\text{Fe}} = 2$, $S_{\text{Nb}} = \frac{1}{2}$, $g_{\text{Co}} = 5.03$, $g_{\text{Fe}} = 2.16$, and $g_{\text{Nb}} = 2$ [54].

-
- [1] J. M. Manriquez, G. T. Yee, R. S. McLean, A. J. Epstein, and J. S. Miller, *Science* **252**, 1415 (1991).
- [2] S. Ferlay, T. Mallah, R. Ouahes, P. Veillet, and M. Verdaguer, *Nature (London)* **378**, 701 (1995).
- [3] S. M. Holmes and G. S. Girolami, *J. Am. Chem. Soc.* **121**, 5593 (1999).
- [4] P. Dechambenoit and J. R. Long, *Chem. Soc. Rev.* **40**, 3249 (2011).
- [5] E. Coronado and G. Minguez Espallargas, *Chem. Soc. Rev.* **42**, 1525 (2013).
- [6] O. Sato, *Nat. Chem.* **8**, 644 (2016).
- [7] D. Pinkowicz, M. Rams, M. Mišek, K. V. Kamenev, H. Tomkowiak, A. Katrusiak, and B. Sieklucka, *J. Am. Chem. Soc.* **137**, 8795 (2015).
- [8] Beata Nowicka, M. Reczyński, M. Rams, W. Nitek, J. Żukrowski, C. Kapusta, and B. Sieklucka, *Chem. Commun.* **51**, 11485 (2015).
- [9] Y. Yoshida, K. Inoue, K. Kikuchi, and M. Kurmoo, *Chem. Mater.* **28**, 7029 (2016).
- [10] J. Milon, M.-C. Daniel, A. Kaiba, P. Guionneau, S. Brandès, and J.-P. Sutter, *J. Am. Chem. Soc.* **129**, 13872 (2007).
- [11] N. Ozaki, H. Tokoro, Y. Hamada, A. Namai, T. Matsuda, S. Kaneko, and S.-i. Ohkoshi, *Adv. Funct. Mater.* **22**, 2089 (2012).
- [12] S.-i. Ohkoshi, S. Takano, K. Imoto, M. Yoshikiyo, A. Namai, and H. Tokoro, *Nat. Photonics* **8**, 65 (2013).
- [13] J. Ferrando-Soria, R. Ruiz-García, J. Cano, S.-E. Stiriba, J. Vallejo, I. Castro, M. Julve, F. Lloret, P. Amorós, J. Pasán, C. Ruiz-Pérez, Y. Journaux, and E. Pardo, *Chem. Eur. J.* **18**, 1608 (2012).
- [14] D. Pinkowicz, R. Podgajny, W. Nitek, M. Rams, A. M. Majcher, T. Nuida, S.-i. Ohkoshi, and B. Sieklucka, *Chem. Mater.* **23**, 21 (2011).
- [15] C. Train, M. Gruselle, and M. Verdaguer, *Chem. Soc. Rev.* **40**, 3297 (2011).
- [16] S. Choraży, R. Podgajny, W. Nitek, T. Fic, E. Gorlich, M. Rams, and B. Sieklucka, *Chem. Commun.* **49**, 6731 (2013).
- [17] C. Train, R. Gheorghe, V. Krstic, L.-M. Chamoreau, N. S. Ovanesyan, G. L. J. A. Rikken, M. Gruselle, and M. Verdaguer, *Nat. Mater.* **7**, 729 (2008).
- [18] C. Train, T. Nuida, R. Gheorghe, M. Gruselle, and S.-i. Ohkoshi, *J. Am. Chem. Soc.* **131**, 16838 (2009).
- [19] S. Choraży, K. Nakabayashi, S.-i. Ohkoshi, and B. Sieklucka, *Chem. Mater.* **26**, 4072 (2014).
- [20] N. A. de Oliveira and P. J. von Ranke, *Phys. Rep.* **489**, 89 (2010).
- [21] E. Fursova, Yu. Shvedenkov, G. Romanenko, V. Ikorskii, and V. Ovcharenko, *Polyhedron* **20**, 1229 (2001).
- [22] E. Yu. Fursova, V. N. Ikorskii, G. V. Romanenko, V. A. Reznikov, Yu. G. Shvedenkov, and V. I. Ovcharenko, *J. Struct. Chem.* **43**, 656 (2002).
- [23] J.-L. Liu, X. Bao, J.-D. Leng, Z.-J. Lin, and M.-L. Tong, *Cryst. Growth Des.* **11**, 2398 (2011).
- [24] S. Choraży, K. Kumar, K. Nakabayashi, B. Sieklucka, and S.-i. Ohkoshi, *Inorg. Chem.* **56**, 5239 (2017).
- [25] C. A. Zimm, A. Jastrab, A. Sternberg, V. K. Pecharsky, K. A. Gschneidner Jr., M. G. Osborn, and I. E. Anderson, *Adv. Cryog. Eng.* **43**, 1759 (1998).
- [26] K. A. Gschneidner, Jr., V. K. Pecharsky, and A. O. Tsokol, *Rep. Prog. Phys.* **68**, 1479 (2005).
- [27] E. Brück, *J. Phys. Appl. Phys.* **38**, R381 (2005).
- [28] O. Tegus, E. Brück, K. H. J. Buschow, and F. R. de Boer, *Nature (London)* **415**, 150 (2002).
- [29] S. A. Nikitin, K. P. Skokov, Y. S. Koshkid'ko, Y. G. Pastushenkov, and T. I. Ivanova, *Phys. Rev. Lett.* **105**, 137205 (2010).
- [30] J.-L. Jin, X.-Q. Zhang, H. Ge, and Z.-H. Cheng, *Phys. Rev. B* **85**, 214426 (2012).
- [31] V. Tkac, A. Orendacova, E. Cizmar, M. Orendac, A. Feher, and A. G. Anders, *Phys. Rev. B* **92**, 024406 (2015).
- [32] H. Zhang, Y. W. Li, E. Liu, Y. J. Ke, J. L. Jin, Y. Long, and B. G. Shen, *Sci. Rep.* **5**, 11929 (2015).
- [33] M. Balli, S. Jandl, P. Fournier, and M. M. Gospodinov, *Appl. Phys. Lett.* **104**, 232402 (2014).
- [34] M. Balli, S. Jandl, P. Fournier, and D. Z. Dimitrov, *Appl. Phys. Lett.* **108**, 102401 (2016).
- [35] K. Engelbrecht, D. Eriksen, C. R. H. Bahl, R. Bjørk, J. Geyti, J. A. Lozano, K. K. Nielsen, F. Saxild, A. Smith, and N. Pryds, *Int. J. Refrig.* **35**, 1498 (2012).

- [36] G. Lorusso, O. Roubeau, and M. Evangelisti, *Angew. Chem., Int. Ed.* **55**, 3360 (2016).
- [37] P. Konieczny, S. Chorąży, R. Pełka, K. Bednarek, T. Wasiutyński, S. Baran, B. Sieklucka, and R. Podgajny, *Inorg. Chem.* **56**, 7089 (2017).
- [38] P. Konieczny, Ł. Michalski, R. Podgajny, S. Chorąży, R. Pełka, D. Czernia, S. Buda, J. Młynarski, B. Sieklucka, and T. Wasiutyński, *Inorg. Chem.* **56**, 2777 (2017).
- [39] P. Konieczny, R. Pełka, D. Czernia, and R. Podgajny, *Inorg. Chem.* **56**, 11971 (2017).
- [40] M. Manoli, R. D. L. Johnstone, S. Parsons, M. Murrie, M. Affronte, M. Evangelisti, and E. K. Brechin, *Angew. Chem. Int. Ed.* **46**, 4456 (2007).
- [41] M. Manoli, A. Collins, S. Parsons, A. Candini, M. Evangelisti, and E. K. Brechin, *J. Am. Chem. Soc.* **130**, 11129 (2008).
- [42] M. Evangelisti and E. K. Brechin, *Dalton Trans.* **39**, 4672 (2010).
- [43] M. Evangelisti, O. Roubeau, E. Palacios, A. Camón, T. N. Hooper, E. K. Brechin, and J. J. Alonso, *Angew. Chem. Int. Ed.* **50**, 6606 (2011).
- [44] J.-L. Liu, Y.-C. Chen, F.-S. Guo, and M.-L. Tong, *Coord. Chem. Rev.* **281**, 26 (2014).
- [45] M. Gajewski, R. Pełka, Y. Miyazaki, M. Fitta, Y. Nakazawa, M. Bałanda, M. Reczyński, B. Nowicka, and B. Sieklucka, *J. Magn. Magn. Mater.* **414**, 25 (2016).
- [46] M. Affronte, A. Ghirri, S. Carretta, G. Amoretti, S. Piligkos, G. A. Timco, and R. E. P. Winpenny, *Appl. Phys. Lett.* **84**, 3468 (2004).
- [47] E. Manuel, M. Evangelisti, M. Affronte, M. Okubo, C. Train, and M. Verdager, *Phys. Rev. B* **73**, 172406 (2006).
- [48] N. Sharma, S. M. Yusuf, A. Kumar, and J. V. Yakhmi, *AIP Conf. Proc.* **1003**, 8 (2008).
- [49] S. M. Yusuf, A. Kumar, and J. V. Yakhmi, *Appl. Phys. Lett.* **95**, 182506 (2009).
- [50] M. Fitta, M. Bałanda, M. Mihalik, R. Pełka, D. Pinkowicz, B. Sieklucka, and M. Zentková, *J. Phys.: Condens. Matter* **24**, 506002 (2012).
- [51] R. Pełka, M. Gajewski, Y. Miyazaki, S. Yamashita, Y. Nakazawa, M. Fitta, D. Pinkowicz, and B. Sieklucka, *J. Magn. Magn. Mater.* **419**, 435 (2016).
- [52] M. Fitta, R. Pełka, M. Bałanda, M. Czapla, M. Mihalik, D. Pinkowicz, B. Sieklucka, T. Wasiutyński, and M. Zentková, *Eur. J. Inorg. Chem.* **2012**, 3830 (2012).
- [53] M. Fitta, M. Bałanda, R. Pełka, P. Konieczny, D. Pinkowicz, and B. Sieklucka, *J. Phys.: Condens. Matter* **25**, 496012 (2013).
- [54] D. Pinkowicz, R. Pełka, O. Drath, W. Nitek, M. Bałanda, A. M. Majcher, G. Poneti, and B. Sieklucka, *Inorg. Chem.* **49**, 7565 (2010).
- [55] R. Pełka, D. Pinkowicz, O. Drath, M. Bałanda, M. Rams, A. Majcher, W. Nitek, and B. Sieklucka, *J. Phys.: Conf. Ser.* **303**, 012037 (2011).
- [56] P. Konieczny, R. Pełka, P. M. Zieliński, F. L. Pratt, D. Pinkowicz, B. Sieklucka, and T. Wasiutyński, *J. Magn. Magn. Mater.* **344**, 105 (2013).
- [57] P. Konieczny, R. Pełka, P. M. Zieliński, T. Wasiutyński, D. Pinkowicz, and B. Sieklucka, *EPJ Web of Conferences* **40**, 14002 (2013).
- [58] R. Pełka, P. Konieczny, P. M. Zieliński, T. Wasiutyński, Y. Miyazaki, A. Inaba, D. Pinkowicz, and B. Sieklucka, *J. Magn. Magn. Mater.* **354**, 359 (2014).
- [59] M. Fitta, R. Pełka, P. Konieczny, and M. Bałanda, *Crystals* **9**, 9 (2019).
- [60] J. Rodríguez-Carvajal, *Physica B* **192**, 55 (1993); the complete program and documentation can be obtained at <https://www.ill.eu/sites/fullprof/>
- [61] M. H. Rietveld, *J. Appl. Cryst.* **2**, 65 (1969).
- [62] See Supplemental Material at <http://link.aps.org/supplemental/10.1103/PhysRevB.104.214428> for arguments against formation of physical mixture, indication of the origins of the misfit of the cobalt and ferrum ions accommodated in the single-crystal structure of CoFeNb, and transition temperatures derived by complementary methods.
- [63] National Nuclear Data Center at Brookhaven National Laboratory: <https://www.nndc.bnl.gov>
- [64] National Institute of Standards and Technology, The NIST Reference on Constants: <https://physics.nist.gov/cuu/Constants/index.html>
- [65] N. J. Stone, *At. Data Nucl. Data Tables* **90**, 75 (2005).
- [66] J. A. Hofmann, A. Paskin, K. J. Tauer, and R. J. Weiss, *J. Phys. Chem. Solids* **1**, 45 (1954).
- [67] J. Wucher and J. D. Wasscher, *Physica* **20**, 721 (1954).
- [68] D. A. Garanin, *Phys. Rev. B* **78**, 020405(R) (2008).
- [69] J. W. Stout and R. C. Chisholm, *J. Chem. Phys.* **36**, 979 (1962).
- [70] H. Suga, M. Sorai, T. Yamanaka, and S. Seki, *Bull. Chem. Soc. Japan* **38**, 1007 (1965).
- [71] M. Sorai, A. Kosaki, H. Suga, and S. Seki, *J. Chem. Thermodynamics* **1**, 119 (1969).
- [72] M. Sorai and S. Seki, *J. Phys. Soc. Jpn.* **32**, 382 (1972).
- [73] M. Majoube, *J. Raman Spectrosc.* **20**, 49 (1989).
- [74] W. S. Benedict, N. Gailar, and E. K. Plyler, *J. Chem. Phys.* **24**, 1139 (1956).
- [75] F. Casanova, X. Batlle, A. Labarta, J. Marcos, L. Manosa, and A. Planes, *Phys. Rev. B* **66**, 212402 (2002).
- [76] A. M. Tishin, A. V. Derkach, Y. I. Spichkin, M. D. Kuz'min, A. S. Chernyshov, K. A. Gschneidner, Jr., and V. K. Pecharsky, *J. Magn. Magn. Mater.* **310**, 2800 (2007).
- [77] H. Oesterreicher and F. T. Parker, *J. Appl. Phys.* **55**, 4334 (1984).
- [78] V. Franco, A. Conde, J. M. Romero-Enrique, and J. S. Blázquez, *J. Phys.: Condens. Matter* **20**, 285207 (2008).
- [79] V. Franco, J. S. Blázquez, and A. Conde, *Appl. Phys. Lett.* **89**, 222512 (2006).
- [80] M. Camprostrini, M. Hasenbusch, A. Pelissetto, P. Rossi, and E. Vicari, *Phys. Rev. B* **65**, 144520 (2002).
- [81] K. A. Gschneidner Jr., V. K. Pecharsky, A. O. Pecharsky, and C. B. Zimm, *Mater. Sci. Forum* **315–317**, 69 (1999).
- [82] K. Szalowski, T. Balcerzak, and A. Bobák, *J. Magn. Magn. Mat.* **323**, 2095 (2011).
- [83] A. Kitanovski and P. W. Egolf, *Int. J. Refrig.* **29**, 3 (2006).
- [84] G. Diguët, G. Lin, and J. Chen, *J. Magn. Magn. Mater.* **350**, 50 (2014).